



Distortional Failure of Cold-Formed Steel Beams under Uniform Bending: Behavior, Strength and DSM Design

André Dias Martins¹, Alexandre Landesmann², Dinar Camotim¹, Pedro Borges Dinis¹

Abstract

This work reports numerical results concerning cold-formed steel simply supported beams buckling and failing in distortional modes under uniform bending and exhibiting three cross-section shapes, namely (i) lipped channels bent about the major-axis, (ii) zed-sections under skew bending causing uniform flange compression (worst case), and (iii) hat-sections subjected to either major-axis or minor-axis bending (compressed lips in the latter case). Two end support conditions are considered, differing only in the warping restraint, which is either null or full. The beams analyzed have several cross-section dimension ratios and lengths, in order to assess their influence on the distortional post-buckling behavior and ultimate strength – particular attention is paid to the influence of (i) the flange-web and lip-flange width ratios, and (ii) the critical (distortional) half-wave number. In addition, the beams exhibit different yield stresses, making it possible to cover wide distortional slenderness ranges. After presenting and discussing the numerical elastic and elastic-plastic post-buckling results obtained, consisting of equilibrium paths, deformed configurations, plastic strain distributions, failure moments and collapse mechanisms, the paper shows that the currently codified Direct Strength Method (DSM) design curve fails to predict adequately the failure moments of some of the beams analyzed and addresses the development/proposal of novel DSM strength curves, providing better quality predictions of all the numerical failure moments available.

1. Introduction

Most cold-formed steel members exhibit slender cross-sections, a feature making them highly prone to several individual (local – L, distortional – D, global – G) or coupled (L-G, L-D, D-G and/or L-D-G) buckling phenomena – in fact, depending on the member geometry and loading, any of these instability phenomena may be critical. It is well known that distortional buckling governs the structural response members with “intermediate lengths”. As far as the distortional failure of cold-formed steel beams is concerned, the research work available includes experimental investigations (*e.g.*, Yu & Schafer 2006, 2007 and Wang & Young 2014), numerical simulations (*e.g.*, Landesmann & Camotim 2016) and design proposals, mainly concerning the development/improvement of Direct Strength Method (DSM)-based approaches (*e.g.*, Schafer & Peköz 1998, Schafer 2008 and Yu & Schafer 2007). Recently, Landesmann & Camotim (2016) provided solid numerical evidence that the currently codified DSM beam distortional

¹ CERIS, ICIST, DECivil, Instituto Superior Técnico, Universidade de Lisboa, Portugal. <andrerdmartins@ist.utl.pt>, <dcamotim@civil.ist.utl.pt> and <dinis@civil.ist.utl.pt>

² Civil Engineering Program, COPPE/UFRJ, Federal University of Rio de Janeiro, Brazil. <alandes@coc.ufrj.br>

design curve (M_{ND}) overestimates the failure moments of lipped channel beams with intermediate-to-high slenderness values. They also showed that the amount of overestimation depends on the beam cross-section geometry (dimension ratios) and end support conditions. Concerning the latter, it is worth noting that the experimental failure moment data used to develop and calibrate the existing DSM distortional strength curve was obtained essentially from 4-point bending tests, which involve uniformly bent beam segments with “warping continuity” conditions at their end cross-sections, *i.e.*, end support conditions lying in-between “free warping” and “prevented warping”. It should also be pointed out that the current M_{ND} curve was calibrated almost exclusively against experimental failure moments of beams with small-to-moderate distortional slenderness ($\lambda_D < 1.5$) – therefore, it is not surprising that this design curve yields quite good estimates within this slenderness range. In summary, the “bias” (in terms of distortional slenderness) of the failure moment data available precluded an adequate calibration in the moderate-to-high distortional slenderness range ($\lambda_D > 1.5$). Fig. 1, adapted from Schafer (2008), plots, against the local or distortional slenderness, the 574 normalized failure moments considered in the development of the current local (M_{NL}) and distortional (M_{ND}) strength curves. In addition, it should be mentioned that these failure moments were obtained from laterally restrained beam tests carried out by 17 researchers and concerning (i) lipped channel beams bent about the major-axis, (ii) zed-section beams under skew bending (about an axis parallel to the flanges) and (iii) hat-section and trapezoidal beams (with or without intermediate stiffeners) bent about the minor-axis. It is still worth noting that, in Fig. 1, one has $\lambda_{max} = (M_y/M_{cr})^{0.5}$, where M_{cr} is the beam critical/lowest (local or distortional) buckling moment – the use of this “mixed slenderness” was due to difficulties in distinguishing between local and distortional failures, due to the bracing and support conditions (Schafer (2008)). These difficulties led Schafer to perform tests on beams designed to exhibit clear local (Yu & Schafer 2003) and distortional (Yu & Schafer 2006) failures. However, the latter beams exhibited again small-to-moderate distortional slenderness values (comprised between 0.68 and 1.53). The above facts led the authors to carry out a detailed investigation on the behavior of uniformly bent cold-formed steel beams exhibiting different cross-sections shapes and failing in pure distortional modes (*i.e.*, unaffected by coupled phenomena involving distortional buckling).

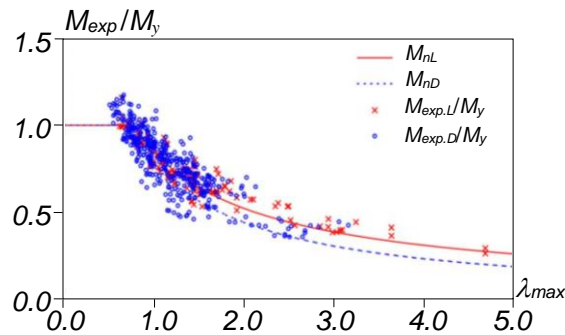


Figure 1: DSM beam local and distortional design curves and experimental local and distortional failure moment data (adapted from Schafer 2008)

This work reports numerical results concerning over 4000 cold-formed steel simply supported beams buckling and failing in distortional modes under uniform bending and exhibiting three cross-section shapes, namely (i) lipped channels bent about the major-axis, (ii) zed-sections under skew bending causing uniform flange compression (worst case), and (iii) hat-sections subjected to either major-axis or minor-axis bending (compressed lips in the latter case) – Fig. 2 shows the various cross-section shapes buckled into beam distortional modes. Two end support conditions are considered, differing in the warping and local displacement/rotation restraints, which are either completely free or fully prevented. The beams analyzed have several cross-section dimension ratios and lengths, in order to assess their

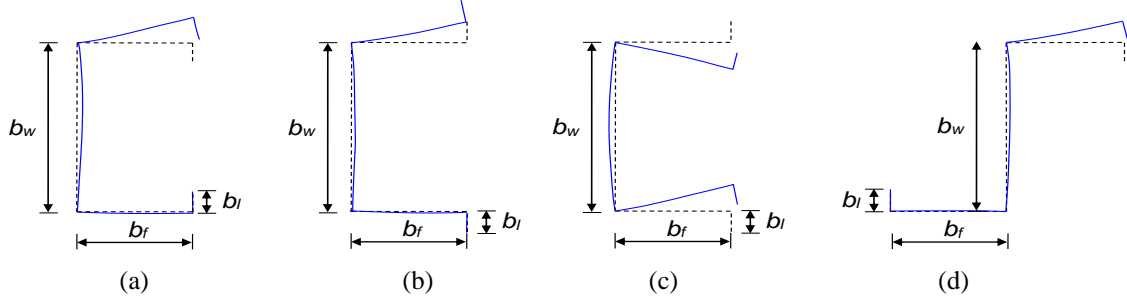


Figure 2: Uniformly bent beam cross-sections buckled in distortional modes: (a) lipped channel (major-axis bending), (b) hat-section (major-axis bending), (c) hat-section (minor-axis bending) and (d) zed-section (skew bending – horizontal neutral axis)

influence on the distortional post-buckling behavior and ultimate strength – particular attention is paid to (i) the web-flange and flange-lip width ratios³, and (ii) the critical (distortional) half-wave number. In addition, the beams have different yield stresses, covering wide slenderness ranges (0.25-4.00 intervals). After presenting and discussing the numerical elastic and elastic-plastic post-buckling results obtained, which consist of equilibrium paths, deformed configurations, plastic strain distributions, failure moments and collapse mechanisms, the paper shows that the currently codified Direct Strength Method (DSM) design curve fails to predict adequately the distortional failure moments of some of the beams analyzed and addresses the development/proposal of novel DSM strength curves, providing better quality predictions of all the numerical failure moments available. Moreover, it will be assessed whether the proposed curves are valid for major and minor-axis bending, like the currently codified DSM beam distortional design curve. Finally, it is still worth noting that the output of this work will be subsequently used in an ongoing research effort aimed at developing rational DSM-based design approaches for cold-formed steel beams affected by L-D interaction, namely the so-called NDL and NLD design approaches (Martins *et al.* 2015), which are based on the beam strength curves concerning individual distortional (and local) failures⁴.

2. Buckling Analysis – Beam Geometry Selection

First of all, it is necessary to identify/select geometries (cross-section dimensions and lengths) of cold-formed steel ($E=210\text{GPa}$, $\nu=0.30$) simply supported beams that buckle and fail in “pure” distortional modes when subjected to uniform bending – since such beams are known to exhibit small-to-moderate distortional post-critical strength reserve, it suffices to find geometries associated with distortional critical buckling (M_{crD}) moments significantly below their local (M_{crL}) and global (M_{crG}) counterparts⁵. As done in previous studies, the beam geometry selection was carried out by means of a “trial-and-error” procedure involving the performance of GBT-based buckling analysis sequences using the code GBTUL (Bebiano *et al.* 2008), taking advantage of its unique modal nature, which makes it possible to obtain buckling moments associated with “pure” local, distortional and global (lateral-torsional) modes. This selection procedure involves four combination of cross-section shape and bending axis, namely (i) lipped channels (C) bent about the major-axis, (ii) zed-sections (Z) under skew bending causing uniform flange compression (worst case), (iii) hat-sections (H_M) bent either about the major-axis and (iv) hat-sections

³ Note that, in the context of columns, Silvestre *et al.* (2005) showed that the cross-section dimensions play an important role in the column distortional post-buckling behavior.

⁴ The most recent results of this ongoing investigation will be reported in the near future (Martins *et al.* 2016).

⁵ In fact, the main difficulty is to preclude the occurrence of interaction with local buckling modes (*i.e.*, L-D interaction), since the selected beams have “reasonably short” lengths. In order to avoid this coupling phenomena, beams with $M_{crL}/M_{crD}>2$ were selected. Nevertheless, it is possible that a few slender beams are still affected by some amount of L-D interaction caused by a “secondary-local bifurcation” – fortunately, such type of L-D interaction has been shown to have a minute impact on the beam failure moment (Martins *et al.* 2015).

(H_m) bent about the minor-axis (lips under compression). In all cases, two end support conditions are considered. The first ones correspond to end cross-section (i) simply supported with respect to major-axis and minor-axis bending, (ii) with the torsional rotations prevented and (iii) free warping displacements and transverse bending rotations – hereafter termed by SCA. As for the second support conditions, hereafter termed SCB, they differ from the first ones in the fact that the warping displacements and transverse bending rotations are fully prevented – physically speaking, these support conditions corresponds to rigidly attaching thick plates to the beam end cross-sections.

The output of this effort are the 30 sets of cross-section dimensions, for each combination of cross-section shape and bending axis, b_w , b_f , b_l , t (web-flange-lip widths and wall thickness – see Fig. 2) and lengths L provided in Annex A (Tables A.1-A.4)⁶. The web-to-flange and flange-to-lip width ratios, as well as the ratios between the critical buckling moments (M_{crI}/M_{crD} and M_{crG}/M_{crD}) are also given in these tables. It is still worth mentioning that the overwhelming majority of the beams selected exhibit single half-wave distortional critical buckling modes. For illustrative purposes, Figs. 3(a)-(c) show the variation of M_{cr} with L (logarithmic scale) for beams C19+SCA, Z8+SCB and H_m 21+SCB, and also the critical (distortional) buckling mode shapes of the beams with the lengths selected.

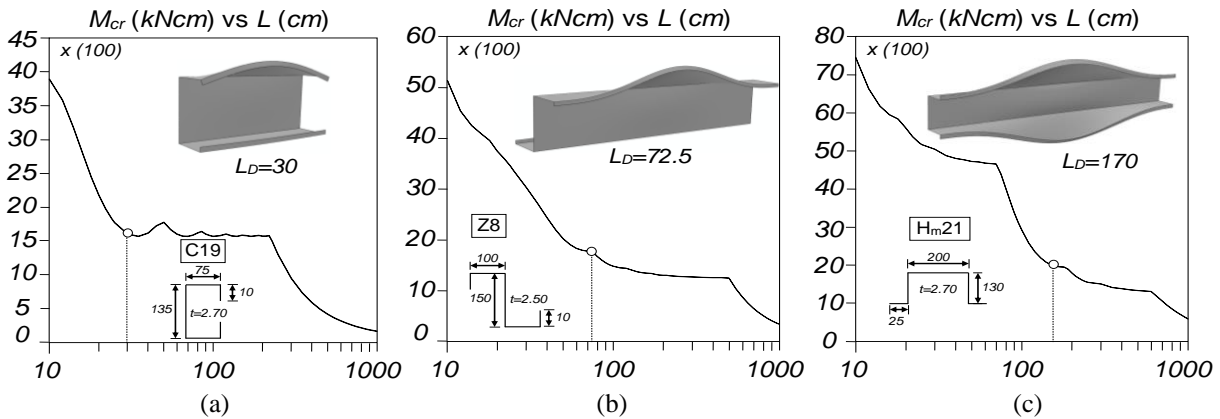


Figure 3: M_{cr} vs. L curves and critical buckling mode shapes of (a) C19+BCA, (b) Z8+BCB and (c) H_m 21+BCB beams

3. Distortional Post-Buckling Behavior

This section presents and discusses relevant numerical results concerning the distortional post-buckling behavior of cold-formed steel beams under uniform bending and, in particular, identifies the key parameters influencing this structural response. After providing a brief description of the shell finite element model adopted, the worst initial geometrical imperfection shape, in the sense that it leads to the lowest strength, is determined for all the beam cases considered in this work. Then, several parametric studies are carried out, in order to assess the influence on the beam behavior, strength and collapse of (i) the change in end support conditions (from SCA to SCB), (ii) the cross-section dimensions, namely the flange-lip and web-flange width ratios, and (iii) the critical buckling mode half-wave number. Finally, all the above behavioral features are addressed in more detail for the hat-section beams under minor-axis bending, since they constitute a problem significantly less studied than the remaining ones.

3.1 Finite Element Modeling

The beam elastic and elastic-plastic post-buckling behaviors were determined by means of ABAQUS (Simulia 2009) shell finite element analyses (SFEA), employing models similar to those used in previous

⁶ For simplicity reasons, the beams with SCA and SCB share the same cross-section dimensions – only the lengths are different.

column studies. Indeed, the only differences concern the loading (bending, instead of axial compression) and support conditions – they consist of (see Martins *et al.* 2015 for a more complete description):

- (I) *Loading*. Equal major-axis (C and H-beams), minor-axis (H-beams) and skew (Z-beams) bending moments are applied at the two end-sections, either (i₁) by means of sets of nodal concentrated forces statically equivalent to 1kNcm (SCA-beams) or (i₂) directly on the rigid end plate centroids (SCB-beams) – Fig. 4 shows SCA and SCB lipped channel beams under uniform major-axis bending.
- (II) *Support Conditions*. The SCA-beams have locally and globally pinned end cross-sections that can warp freely and are prevented from twisting. These support conditions were modelled by imposing null transverse displacements (along the X and Y axes – see Fig. 4(a)) at the end cross-sections and, in order to avoid numerical difficulties related to the load application, both end cross-sections are free to move axially (the axial rigid-body translation is precluded by preventing the axial (along Z) displacement of the mid-span mid-web point). As for the SCB-beams, their end cross-sections are attached to rigid plates, thus ensuring full warping and local displacement/rotation restraint, whose external surfaces rest on spherical hinges that are prevented from twisting (Camotim & Dinis 2013) – see Fig. 4(b), showing also an end support detail⁷. Therefore, the beam end cross-sections are locally fixed and globally pinned (simply supported).

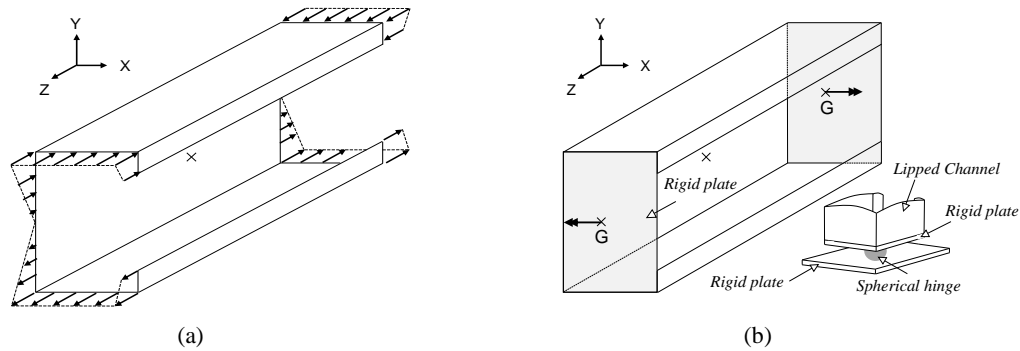


Figure 4: End support and loading conditions of beams with (a) SCA and (b) SCB end support conditions.

3.2 Initial Geometrical Imperfections

Since it is well known that the initial geometrical imperfection shape always plays a crucial role in the non-linear behavior of thin-walled cold-formed steel members, it is essential to determine the most detrimental critical buckling mode shape, *i.e.*, that leading to the lowest beam strength and failure moment. In this context, it is worth recalling that Prola & Camotim (2002) unveiled a non-negligible beam distortional post-buckling asymmetry, with respect to the cross-section distortion “sign” (*i.e.*, outward or inward compressed flange-lip motions). In order to confirm/illustrate this finding, Fig. 5(a) shows the elastic post-buckling equilibrium paths M/M_{crD} vs. $(v+v_0)/t$ (v is the mid-span top flange-lip corner vertical displacement and v_0 is the corresponding imperfection/initial value) of C19+SCA beams⁸ containing “pure” distortional initial imperfections with both “signs”, sharing the same amplitude $0.1t$. The observation of these post-buckling results prompts the following comments:

⁷ Note that the spherical hinges are deemed attached to the rigid end plates through an arrangement (not shown) that prevents twisting.

⁸ This procedure was conducted for all the remaining five beam types considered (*i.e.*, C+SCB, H_m+SCA, H_m+SCB, Z+SCA and Z+SCB). However, due to space limitation, no results and figures are presented for these cases – nevertheless, it should be mentioned that the same tendency was observed (the distortional initial imperfection involving inward compressed flange-lip motions is the most detrimental). The H_m+SCA and H_m+SCB beam types will be addressed in Section 3.6.

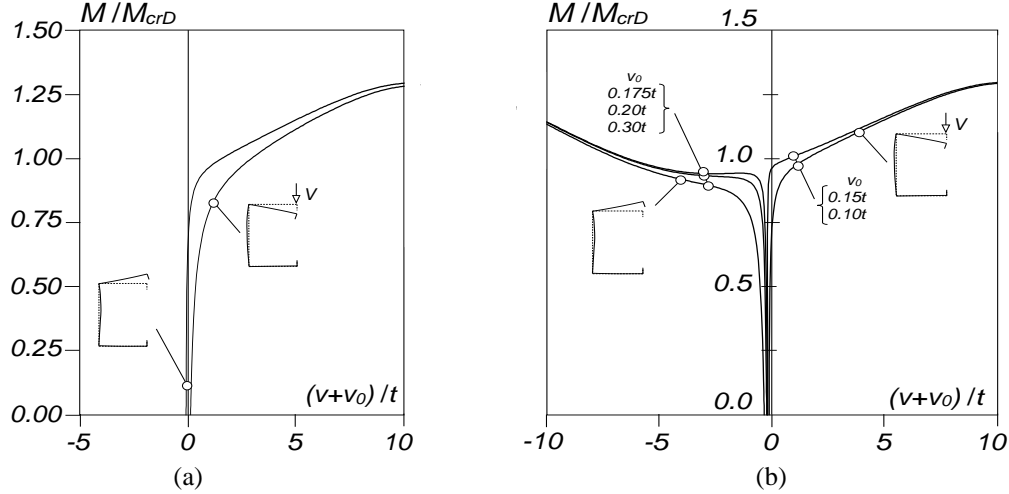


Figure 5: Imperfection sensitivity study (C19+SCA beams): elastic post-buckling equilibrium paths M/M_{crD} vs. $(v+v_0)/t$ for beams with (a) inward and outward initial imperfections and (b) outward initial imperfections with various amplitudes

- (i) The inward equilibrium path always lies below its outward counterpart, which means that the corresponding initial imperfection shape is the most detrimental (leads to the lowest strength).
- (ii) The outward equilibrium path exhibits inward top flange-lip motions in the pre-buckling stages. Dinis & Camotim (2010) showed that this quite surprising behavior stems from the occurrence of flange curling (*e.g.*, Bernard *et al.* 1996), which means that the final nature ($v > 0$ or $v < 0$) of the outward equilibrium path is the result of a balance between two opposing tendencies: (ii₁) an outward one, due to the initial imperfection shape, and (ii₂) an inward one, due to the flange curling effect – of course, this implies the existence of a “limit imperfection amplitude”, associated with a “nature switch”. Fig. 5(b) shows M/M_{crD} vs. $(v+v_0)/t$ equilibrium paths concerning beams containing five outward initial imperfections with amplitudes varying between $0.10t$ and $0.30t$. It can be readily seen that the “limit imperfection amplitude” lies between $0.15t$ and $0.175t$ – note that the equilibrium path associated with $0.10t$ has also been depicted in Fig. 5(a). Moreover, there is a clear distortional asymmetry with respect to the imperfection “sign”, as first unveiled by Prola & Camotim (2002).

3.3 Influence of the Support Conditions

The influence of the end support conditions (SCA and SCB) on the distortional post-buckling behavior of (simply supported) is addressed in this section – a C-beam geometry was chosen to illustrate this influence, namely $b_w=200$, $b_f=100$, $b_r=10$, $t=2.5$ and $L=450$ (mm). Fig. 6(a) shows several post-buckling equilibrium paths (elastic and elastic-plastic) M/M_{crD} vs. $(v+v_0)/t$ concerning beams with the above geometry and support conditions SCA and SCB, both containing distortional initial imperfections involving inward compressed flange-lip motions (the most detrimental shape, as shown earlier) with a $0.1t$ amplitude. On the other hand, Fig. 6(b) shows deformed configurations and plastic strains on the onset of collapse of the two beams exhibiting yield stresses corresponding to $\lambda_D=1.0$, 2.5 and 3.5 – note that the $\lambda_D=1.0$ beam displacements are amplified 2 times. The observation of these figures shows that:

- (i) The SCB beams exhibit a much more pronounced distortional post-buckling strength than their SCA counterparts, which stems essentially from the end support warping fixity – for instance, note the difference between the elastic equilibrium path tangent stiffness values for $M/M_{crD} > 1.0$. Moreover, the SCB beams also exhibits a higher elastic-plastic strength reserve (and ductility) than the SCA beams – the failure moments of the latter are reached almost simultaneously with the onset of yield, occurring after a fairly smooth fast continuous elastic stiffness erosion/degradation.

- (ii) As intended, all beams exhibit typically distortional failure configurations, which are akin to the initial geometrical imperfection shape. The failure modes of the two sets of beams (see Fig. 6(b)) are qualitatively similar and associated with the yielding of the mid-span compressed flange-web corner and lip free edge regions (*i.e.*, plastic strain distributions typically occurring at distortional collapses). The exceptions are the stocky beams ($\lambda_D=1.0$), which collapse abruptly under “almost uniform”

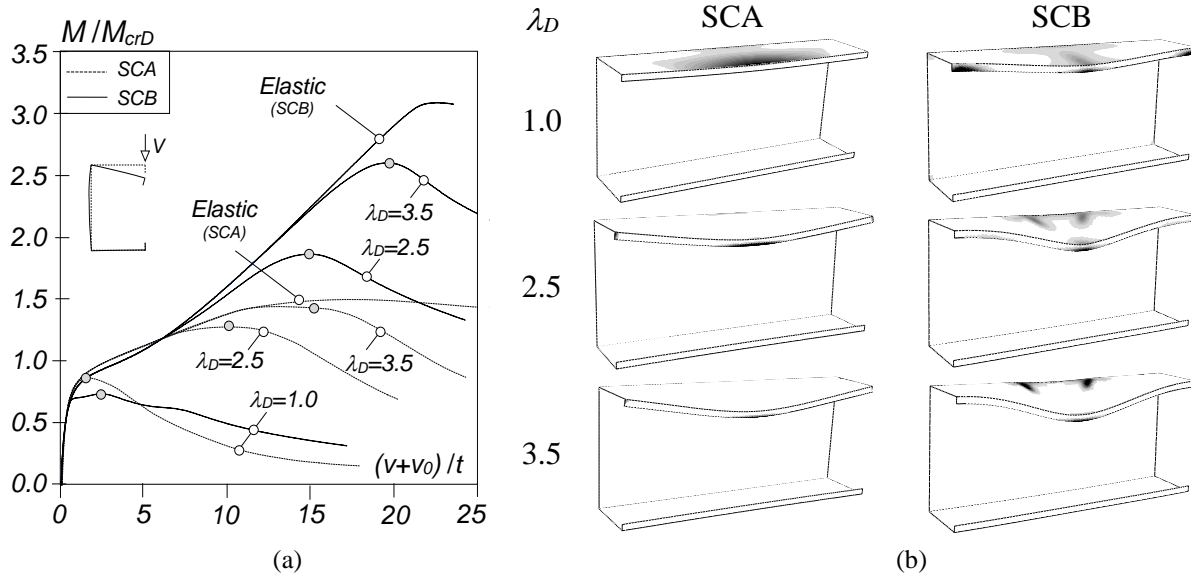


Figure 6: (a) Elastic and elastic-plastic post-buckling equilibrium paths M/M_{crD} vs. $(v+v_0)/t$ for beams with identical cross-section dimensions and distinct boundary conditions (b) failure modes and plastic strains for $\lambda_D=1.0, 2.5, 3.5$

- (ii) As intended, all beams exhibit typically distortional failure configurations, which are akin to the initial geometrical imperfection shape. The failure modes of the two sets of beams (see Fig. 6(b)) are qualitatively similar and associated with the yielding of the mid-span compressed flange-web corner and lip free edge regions (*i.e.*, plastic strain distributions typically occurring at distortional collapses). The exceptions are the stocky beams ($\lambda_D=1.0$), which collapse abruptly under “almost uniform” normal stress distributions. Although not shown here, the plastic strain distributions in the descending branch are characterized by further spread of plasticity, leading to the formation of a “distortional plastic hinge” in the beam mid-span region (see Martins *et al.* 2015).
- (iii) Surprisingly, the elastic equilibrium paths depicted in Fig. 6(a) show that, for $0.5 < M/M_{crD} < 1.2$, the SCA beam exhibits a marginally higher normalized strength than its SCB counterpart. A close observation of the $\lambda_D=1.0$ SCB beam collapse mechanism shows stress concentrations near the end cross-sections (see Fig. 6(b)), due to fairly short length, which is responsible for the above decrease in normalized strength. In order to confirm this assertion, a similar study was conducted with longer beams (buckling in modes exhibiting two distortional half-waves), and it was concluded that the SCB beam is always stiffer than its SCA counterpart (as expected) – these results are not show here.

3.4 Influence of the Cross-Section Dimensions

3.4.1 Ratio b_f/b_l

In order to assess the influence of the flange-lip width ratio b_f/b_l on the behavior and ultimate strength of uniformly bent beams, this section presents and discusses results concerning C+SCA and H_M+SCB beams with the same web-flange width ratio (b_w/b_f), equal to 1.25 ($b_w=150$, $b_f=120$, $t=3.5$ and $L=420$ mm or $L=700$ mm for the C and H_M beams, respectively) and 2.0 ($b_w=200$, $b_f=100$, $t=2.5$ and $L=450$ mm

or $L=700\text{mm}$ for the C and H_M beams, respectively), both having three b_f/b_l ratios⁹, namely 12, 10 and 8. Figs. 7(a₁)-(c₂) show elastic and elastic-plastic equilibrium paths M/M_{crD} vs. $(v+v_0)/t$ of C+SCA ($b_w/b_f=2.0$ and three b_f/b_l values¹⁰ – Figs. 7(a₁)-(c₁)) and H_M +SCB ($b_w/b_f=2.0$ and three b_f/b_l values⁹ – Fig. 7(a₂)-(c₂)) beams. From the observation of these figures it can be readily conclude that:

- (i) The ratio b_f/b_l plays an important role in the beam distortional post-buckling behavior ultimate strength of beams, as can be attested by looking at Figs. 7(a₁)-(c₂): a b_f/b_l decrease causes a drastic M_U/M_{crD} reduction – the comparison between the tangent stiffness values of the C+SCA (Figs. 7(a₁)-(c₁)) and H_M +SCB (Figs. 7(a₂)-(c₂)) beam elastic equilibrium paths reinforces this conclusion – in the former, the elastic limit point occurs for gradually smaller M_U/M_{crD} values as b_f/b_l decreases.
- (ii) In order to quantify the ultimate strength reduction/variation, Table 1 shows the M_U/M_{crD} and M_U/M_y values for C+SCA and H_M +SCB beams exhibiting all combinations of (ii₁) $\lambda_D=1.0, 2.5, 3.5$ (ii₂) $b_w/b_f=1.25, 2.0$ and (ii₃) $b_f/b_l=12, 10, 8$. This table shows that, for constant b_w/b_f and λ_D , M_U/M_{crD} and M_U/M_y decrease with b_f/b_l . For instance, in the C+SCA-beam with $b_w/b_f=1.25$ the ratio M_U/M_{crD} decreases 29% when the b_f/b_l varies from 12 to 8. Naturally, such differences will entail a

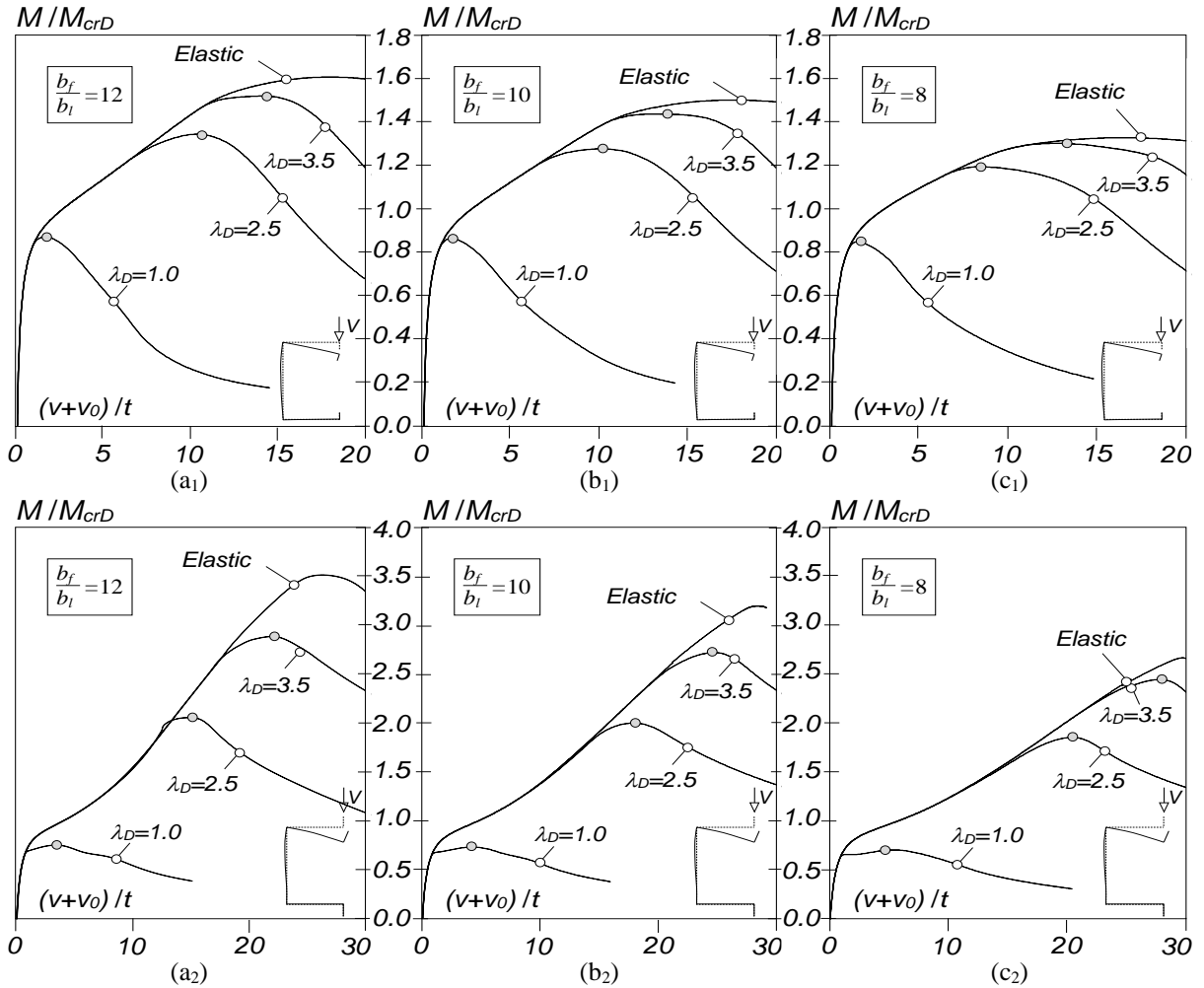


Figure 7: M/M_{crD} vs. $(v+v_0)/t$ equilibrium paths for (1) C+SCA and (2) H_M +SCB beams with b_f/b_l ratios equal to (a) 12, (b) 10 and (c) 8

⁹ For simplicity purposes, the flange width is kept constant and only the lip width varies.

¹⁰ Since the results obtained for the beams with $b_w/b_f=1.25$ are qualitatively similar to those presented, they have been omitted from the paper.

Table 1: Influence of b_f/b_l on the beam ultimate strength for different (i) distortional slenderness and (ii) b_w/b_f values

Beam	$\frac{b_w}{b_f}$	λ_D	$\frac{b_f}{b_l} = 12$		$\frac{b_f}{b_l} = 10$		$\frac{b_f}{b_l} = 8$	
			M_U/M_y	M_U/M_{crD}	M_U/M_y	M_U/M_{crD}	M_U/M_y	M_U/M_{crD}
C+SCA	1.25	1.0	0.835	0.835	0.827	0.827	0.811	0.811
		2.5	0.207	1.291	0.191	1.192	0.174	1.085
		3.5	0.134	1.638	0.121	1.486	0.095	1.169
	2.00	1.0	0.868	0.868	0.861	0.861	0.840	0.840
		2.5	0.214	1.335	0.203	1.271	0.189	1.183
		3.5	0.124	1.515	0.108	1.328	0.105	1.292
H _M +SFB	1.25	1.0	0.718	0.718	0.685	0.685	0.643	0.643
		2.5	0.337	2.104	0.310	1.935	0.275	1.721
		3.5	0.244	2.991	0.220	2.700	0.178	2.179
	2.00	1.0	0.735	0.735	0.718	0.718	0.695	0.695
		2.5	0.323	2.018	0.315	1.970	0.292	1.823
		3.5	0.231	2.831	0.219	2.682	0.196	2.402

“vertical dispersion” of the whole set of M_U/M_y values corresponding to a given λ_D – recall that the DSM distortional strength curve depends solely on λ_D .

3.4.2 Ratio b_w/b_f

Attention is now turned to assessing the impact of the web-flange width ratio b_w/b_f on the beam behavior and ultimate strength (keeping all other dimensions unchanged). C+SCA ($b_f=100$, $b_l=10$, $t=2.5$ and $L=450$ mm) and Z+SCB-beams ($b_f=100$, $b_l=10$, $t=3.0$ and $L=700$ mm) beams are now analyzed, for b_w/b_f values equal to 2.0 ($b_w=200$ and $b_f=100$), 2.5 ($b_w=250$ and $b_f=100$) and 3.0 ($b_w=300$ and $b_f=100$). Figs. 8(a₁)-(c₂) show their elastic and elastic-plastic equilibrium paths M/M_{crD} vs. $(v+v_0)/t$ (the latter for $\lambda_D=1.0, 2.5, 3.5$). On the other hand, Table 2 provides the M_U/M_{crD} and M_U/M_y values of the above beams. The observation of these results prompts the following remarks:

- (i) The ratio b_w/b_f plays a minute role in the distortional post-buckling behavior and ultimate strength, of the two beam types, as clearly demonstrated by the M_U/M_{crD} and M_U/M_y values given in Table 2 and the equilibrium paths depicted in Figs. 8(a₁)-(c₁) and 8(a₂)-(c₂). Nevertheless, it is possible to observe the following tendency: M_U/M_{crD} and M_U/M_y (slightly) increase when b_w/b_f increases.
- (ii) The comparison between influences of the ratios b_f/b_l (previous section) and b_w/b_f (this section), clearly show that the former plays a much more important role in the ultimate strength of beams undergoing distortional collapses.

3.5 Critical Buckling Mode Half-Wave Number

The last parameter whose influence on the beam behavior and ultimate strength is going to be assessed is the (distortional) critical buckling mode half-wave number n_D . To illustrate this influence, two C+SCB beams are analyzed, exhibiting the same cross-section dimensions ($b_w=200$, $b_f=100$, $b_l=10$ and $t=2.5$ mm) and having lengths $L=770$ mm and $L=1200$ mm, corresponding to critical buckling modes with one and two distortional half-waves, respectively. Once again, Figs. 9(a₁)-(a₂) show elastic and elastic-plastic equilibrium paths M/M_{crD} vs. $(v+v_0)/t$ of beams with $\lambda_D=1.0, 2.5, 3.5$ – v is either the mid-span top flange-lip corner vertical displacement ($n_D=1$) or the most inward flange-lip corner vertical displacement ($n_D=2$). Moreover, Figs. 9(b₁)-(b₂) show the deformed configurations, at the onset of collapse, of the above beams and Table 3 provides their M_U/M_{crD} and M_U/M_y values. Observing these post-buckling results shows that:

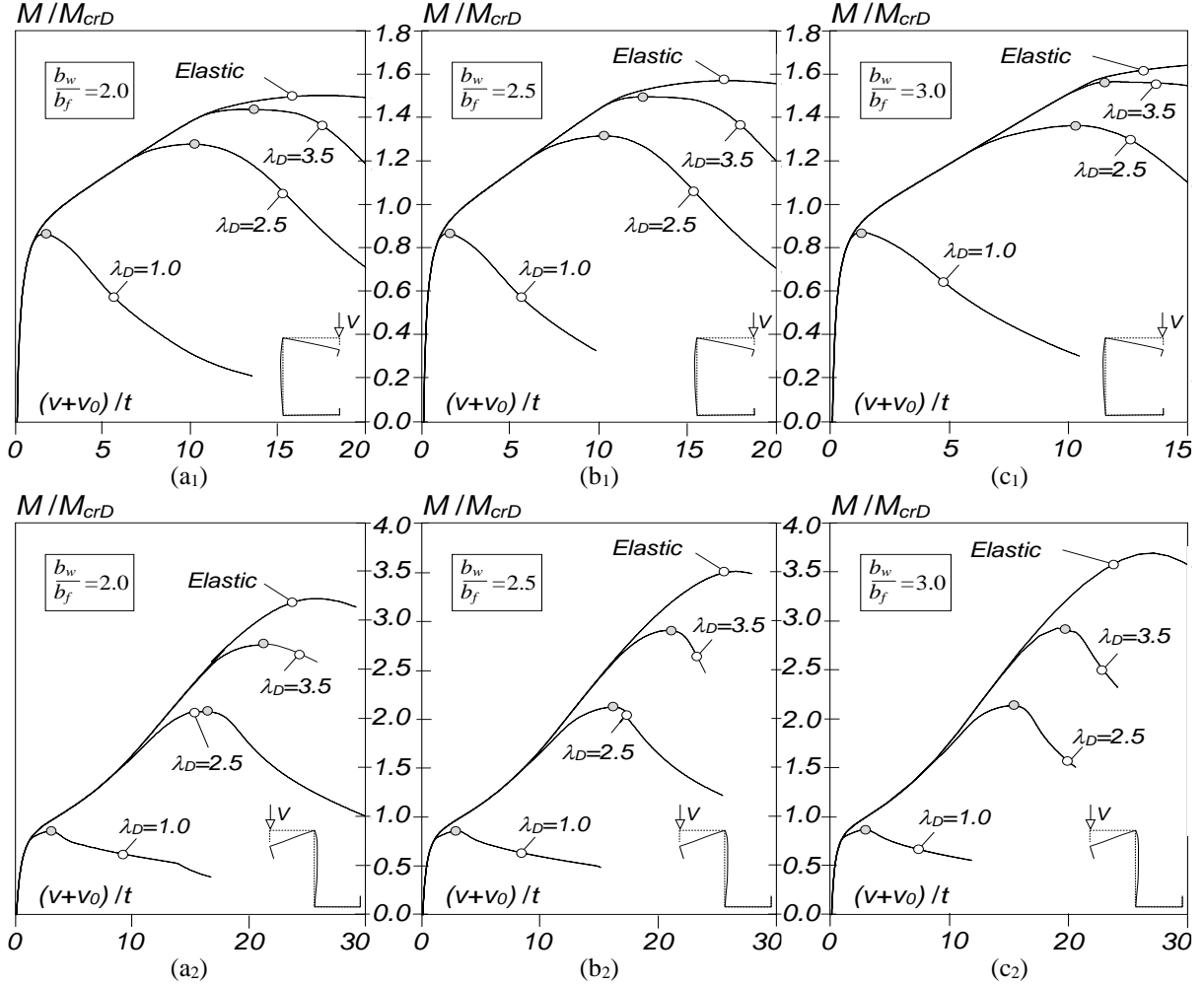


Figure 8: M/M_{crD} vs. $(v+v_0)/t$ equilibrium paths for (i) C+SCA and (ii) Z+SCB beams with b_w/b_f ratios equal to (a) 2.0, (b) 2.5 and (c) 3.0

Table 2: Influence of b_w/b_f on the beam ultimate strength for different distortional slenderness values

Beam	λ_D	$\frac{b_w}{b_f} = 2.0$		$\frac{b_w}{b_f} = 2.5$		$\frac{b_w}{b_f} = 3.0$	
		M_U/M_y	M_U/M_{crD}	M_U/M_y	M_U/M_{crD}	M_U/M_y	M_U/M_{crD}
C+SCA	1.0	0.859	0.859	0.864	0.864	0.864	0.864
	2.5	0.203	1.271	0.209	1.308	0.216	1.351
	3.5	0.108	1.327	0.122	1.490	0.127	1.552
Z+SCB	1.0	0.835	0.835	0.843	0.843	0.851	0.851
	2.5	0.325	2.032	0.335	2.093	0.336	2.102
	3.5	0.220	2.696	0.234	2.862	0.236	2.889

- (i) The evolutions of the plastic strains along the equilibrium paths, up to collapse, of the $L=770\text{mm}$ ($n_D=1$) beams follow the trends exhibited by the C+SCB beams analyzed in Section 3.3.
- (ii) The observation of Figs. 9(b₁)-(b₂) readily shows the similarities between the $\lambda_D=2.5$ and $\lambda_D=3.5$ beam failure mechanisms: both are associated with the yielding of the lip free edge and web-flange corner regions. However, the longitudinal location of such regions is different: mid-span, for the $n_D=1$ beam, and crest of the inward half-wave, for $n_D=2$ beam.

Table 3: Influence of the critical buckling mode half-wave number on the C+SCB beam ultimate strength ($\lambda_D = 1.0, 2.5, 3.5$)

Beam	λ_D	$n_D = 1$		$n_D = 2$	
		M_U/M_y	M_U/M_{crD}	M_U/M_y	M_U/M_{crD}
C+SCB	1.0	0.813	0.813	0.811	0.811
	2.5	0.279	1.744	0.259	1.621
	3.5	0.195	2.395	0.166	2.030

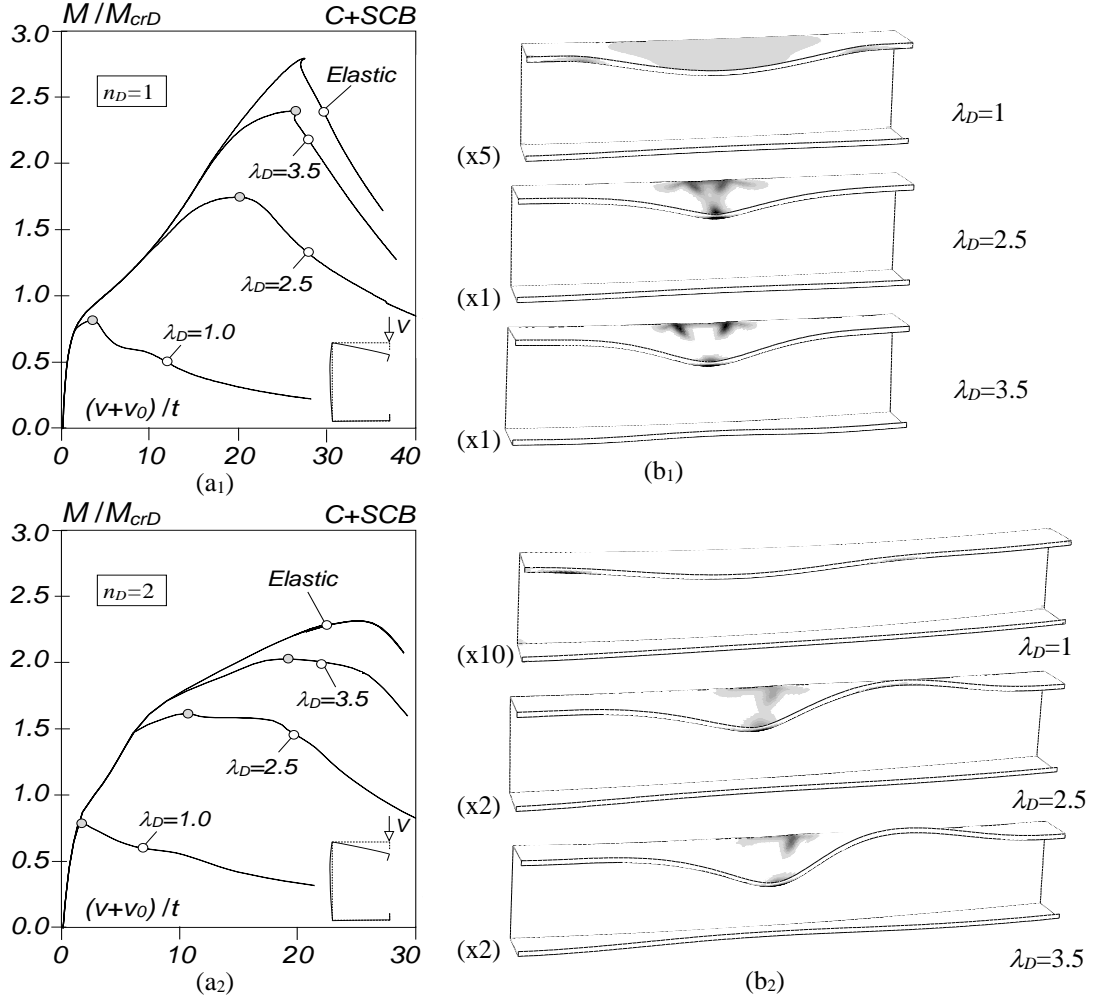


Figure 9: (a) M/M_{crD} vs. $(v+v_0)/t$ equilibrium paths M/M_{crD} vs. $(v+v_0)/t$ of C+SCB beams with one $n_D=1$ ($L=770\text{mm}$) and $n_D=2$ ($L=1200\text{mm}$), and (b) failure modes and plastic strain distributions of such beams with $\lambda_D=1.0, 2.5, 3.5$

- (iii) The M_U/M_{crD} and M_U/M_y values provided in Table 3 show that the critical buckling mode half-wave number also plays an important role in the ultimate strength of beams failing in distortional modes, particularly those with high slenderness values. For instance, for $\lambda_D=3.5$ the M_U/M_y and M_U/M_{crD} values decrease from 0.195-2.395 to 0.166-2.030 when n_D increase from 1 to 2.
- (iv) Naturally, beams can also buckle in modes exhibiting three or more half-waves. However, this only occurs for beams with lengths for which, at least under uniform bending, it is very rare to find “pure” distortional collapse – indeed, interaction with local buckling is bound to take place (“secondary local bifurcation L-D interaction” – Martins *et al.* 2015), a phenomenon outside the scope of this work.

3.6 Hat-Sections Beams under Minor-Axis Bending

This section deals with hat-section SCB beams subjected to uniform minor-axis bending (H_m +SCB beams) and goes over all the topics addressed previously, namely (i) the initial geometrical imperfections, (ii) the influence of the cross-sections dimensions and (iii) the influence of the critical buckling mode half-wave number. Figs. 10(a)-(b) show the elastic and elastic-plastic ($\lambda_D=1.0, 2.5, 3.5$) post-buckling equilibrium paths M/M_{crD} vs. $(v+v_0)/t$ of H_1 +SCB (see Table A.4) containing inward and outward “pure” distortional initial imperfections, both with amplitude $0.1t$ – Fig. 10(c) shows deformed configurations of the elastic-plastic beams. On the other hand, Figs. 11(a)-(c) show elastic elastic-plastic M/M_{crD} vs. $(v+v_0)/t$ equilibrium paths of beams with $b_w=120$, $t=2.5$ and $L=500$ mm, and three b_f/b_l ratios, namely 3 ($b_f=55$ mm and $b_l=18.3$ mm), 5 ($b_f=60$ mm and $b_l=12$ mm) and 7 ($b_f=60$ mm and $b_l=8.57$ mm), in order to assess its influence on the beam ultimate strength. Similarly, Figs. 12(a)-(c), intended to assess the influence of the web-flange width ratio, shows M/M_{crD} vs. $(v+v_0)/t$ equilibrium paths for beams with $b_f=60$, $b_l=10$, $t=2.5$ and $L=500$ mm, and three b_w/b_f values: 1.0 ($b_w=60$ mm), 1.50 ($b_w=90$ mm) and 2.0 ($b_w=120$ mm). Finally, Figs. 13(a)-(c) assess the impact of the critical buckling mode half-wave number on the load-carrying capacity of the H_m +SCB beams – they shows the M/M_{crD} vs. $(v+v_0)/t$ equilibrium paths of beams with

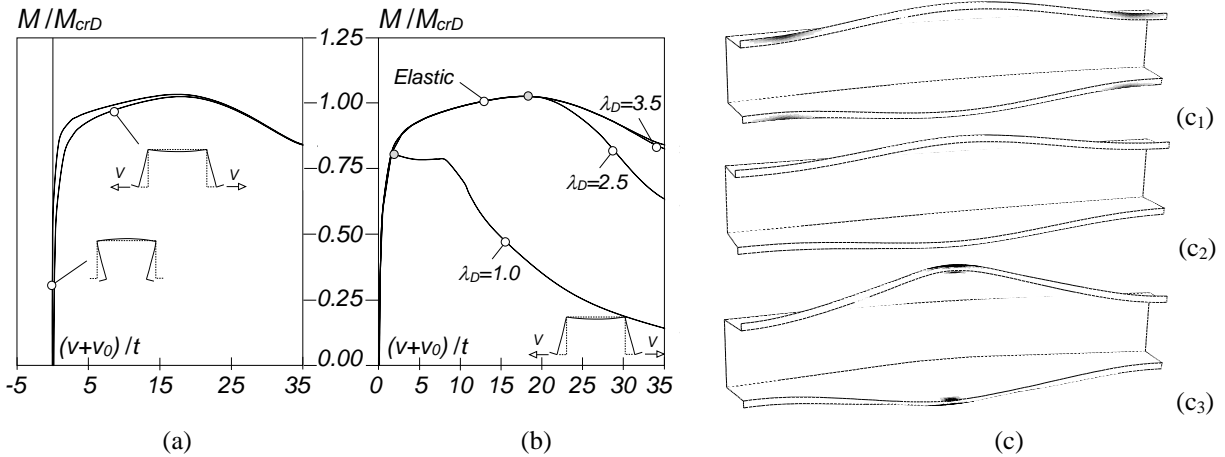


Figure 10: H_m +SCB beams: (a) elastic and (b) elastic-plastic ($\lambda_D=1.0, 2.5, 3.5$) M/M_{crD} vs. $(v+v_0)/t$ equilibrium paths, and (c) deformed configurations at failure for (1) $\lambda_D=1.0$ and (2) $\lambda_D=2.5=3.5$, and (3) at $(v+v_0)/t=35$

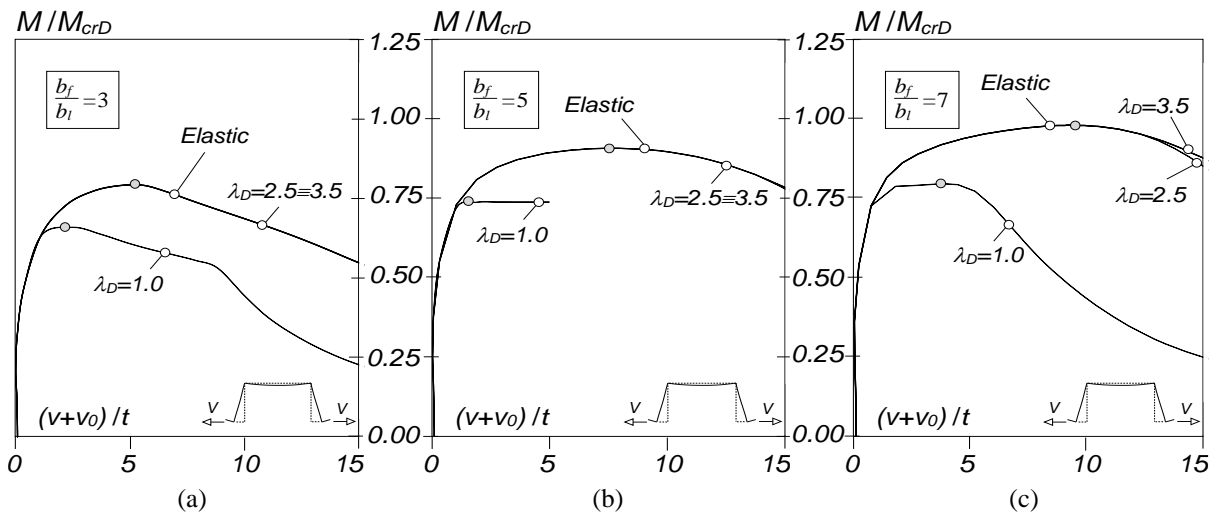


Figure 11: H_m +SCB beams: elastic and elastic-plastic ($\lambda_D=1.0, 2.5, 3.5$) M/M_{crD} vs. $(v+v_0)/t$ equilibrium paths for b_f/b_l equal to (a) 3, (b) 5 and (c) 7

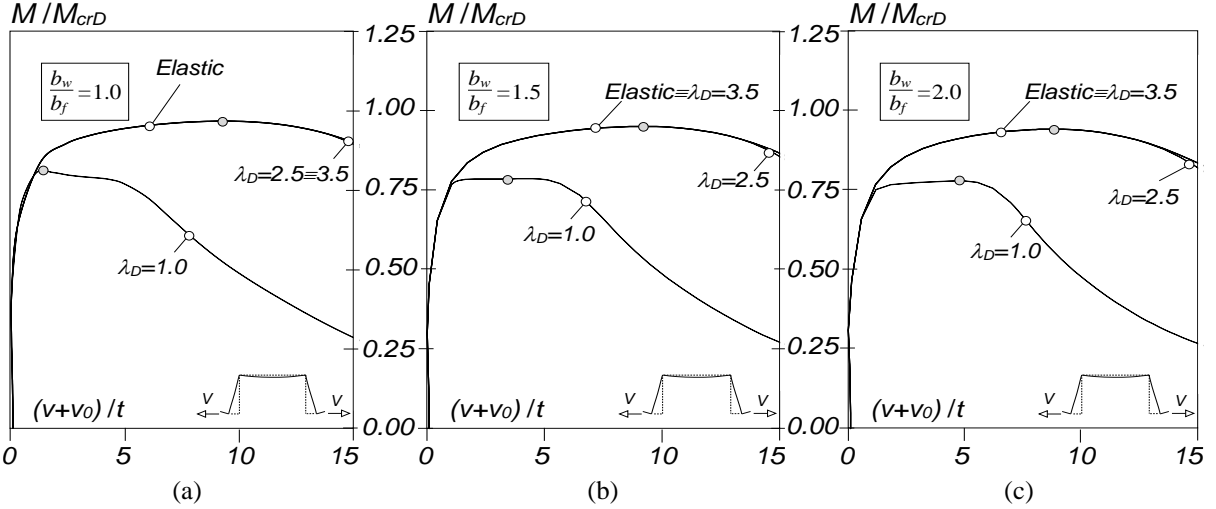


Figure 12: H_m+SCB beams: elastic and elastic-plastic ($\lambda_D=1.0, 2.5, 3.5$) M/M_{crD} vs. $(v+v_0)/t$ equilibrium paths for b_w/b_f equal to (a) 1.0, (b) 1.5 and (c) 2.0

$b_w=120\text{mm}$, $b_f=60\text{mm}$, $b_l=12\text{mm}$ and $t=2.5\text{mm}$, and $L=500\text{mm}$ ($n_D=1$), $L=1000\text{mm}$ ($n_D=2$) and $L=1300\text{mm}$ ($n_D=3$). The observation of all these results prompts the following comments:

- (i) Fig. 10(a) shows that (i1) the outward initial imperfections are the most detrimental and (i2) the “inward equilibrium path” exhibits outward flange-lip motions in the pre-buckling stages – these observations are opposite to those made in the context of major-axis bending (see Section 3.2).
- (ii) Fig. 10(b) depicts the elastic-plastic equilibrium paths, corresponding to beams with $\lambda_D=1.0, 2.5, 3.5$ and containing the most detrimental initial imperfections. It is readily observed that the $\lambda_D=2.5, 3.5$ beams fail in the elastic range (Fig. 10(c2)), after a smooth continuous stiffness erosion/degradation – plasticity only occurs in the descending branch, at the mid-span lip free edge regions – see Fig. 10(c3). As for the $\lambda_D=1.0$ beam, the yield and failure moments practically coincide – see Fig. 10(c1).
- (iii) The flange-lip width ratio also plays an important role in the distortional post-buckling behavior of hat-section beams bent about the minor-axis, as can be attested by looking at Figs. 11(a)-(c) – the failure moment increases with the ratio b_f/b_l . Table 4 quantifies this relation: e.g., for $\lambda_D=3.5$, M_U/M_y

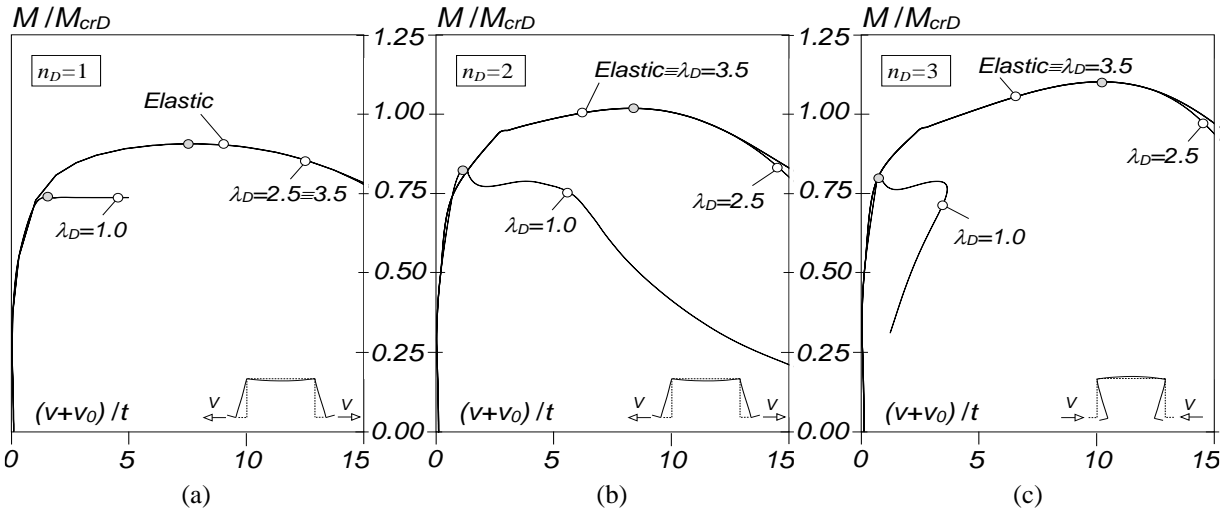


Figure 13: H_m+SCB beams: elastic and elastic-plastic ($\lambda_D=1.0, 2.5, 3.5$) M/M_{crD} vs. $(v+v_0)/t$ equilibrium paths of beams with (a) $n_D=1$ ($L=500\text{mm}$), (b) $n_D=2$ ($L=1000\text{mm}$) and (c) $n_D=3$ ($L=1300\text{mm}$)

Table 4: Influence of the ratio b_f/b_l on the failure moment of ultimate strength of H_m +SCB beams with $\lambda_D=1.0, 2.5, 3.5$

Beam	λ_D	$\frac{b_f}{b_l} = 3$		$\frac{b_f}{b_l} = 5$		$\frac{b_f}{b_l} = 7$	
		M_U/M_y	M_U/M_{crD}	M_U/M_y	M_U/M_{crD}	M_U/M_y	M_U/M_{crD}
H_m +SCB	1.0	0.660	0.660	0.737	0.737	0.794	0.794
	2.5	0.127	0.793	0.145	0.906	0.156	0.977
	3.5	0.065	0.793	0.074	0.906	0.080	0.977

Table 5: Influence of the ratio b_w/b_f on the failure moment of ultimate strength of H_m +SCB beams with $\lambda_D=1.0, 2.5, 3.5$

Beam	λ_D	$\frac{b_w}{b_f} = 1.0$		$\frac{b_w}{b_f} = 1.5$		$\frac{b_w}{b_f} = 2.0$	
		M_U/M_y	M_U/M_{crD}	M_U/M_y	M_U/M_{crD}	M_U/M_y	M_U/M_{crD}
H_m +SCB	1.0	0.805	0.805	0.788	0.788	0.781	0.781
	2.5	0.154	0.965	0.152	0.953	0.151	0.943
	3.5	0.079	0.965	0.078	0.953	0.077	0.943

Table 6: Influence of the critical buckling mode half-wave number on the failure moment H_m +SCB beams with $\lambda_D=1.0, 2.5, 3.5$

Beam	λ_D	$n_D = 1$		$n_D = 2$		$n_D = 3$	
		M_U/M_y	M_U/M_{crD}	M_U/M_y	M_U/M_{crD}	M_U/M_y	M_U/M_{crD}
H_m +SCB	1.0	0.737	0.737	0.821	0.821	0.803	0.803
	2.5	0.145	0.906	0.163	1.018	0.177	1.105
	3.5	0.074	0.906	0.083	1.018	0.090	1.105

increases from 0.065 ($b_f/b_l=3$) to 0.074 (+14%) ($b_f/b_l=5$) and to 0.080 (+23%) ($b_f/b_l=7$). On the other hand, the web-flange width ratio plays again a minute role (see Figs. 12(a)-(c) and Table 5). The M_U/M_y and M_U/M_{crD} values are practically constant for a given λ_D – rigorously speaking, they slightly decrease with b_w/b_f (unlike in the beams bent about the major-axis).

- (iv) Finally, Figs. 13(a)-(c) and Table 6 show the influence of the critical buckling mode half-wave number on the beam ultimate strength: when n_D increases, the M_U/M_y and M_U/M_{crD} values also increase (unlike in the beams bent about the major-axis). For instance, the ratio M_U/M_y , which may be viewed as associated with the DSM distortional curve, increases from 0.074 to 0.090 (+21%) when the beam buckling mode half-wave number grows from 1 to 3.

Before concluding this numerical investigation, it is worth recalling the following observations:

- (i) The initial geometrical imperfections, end support boundary conditions, flange-lip width ratio and critical buckling mode half-wave number play an important role in the beam post-buckling behavior and ultimate strength – conversely, the web-flange width ratio has a minute/negligible influence.
- (ii) Two approaches can be adopted for the proposal of DSM-based distortional curves (ii₁) the first one by considering all the parameters identified in the item above into a single expression and (ii₂) the second, by maintaining the philosophy inherent to the DSM, *i.e.*, depending solely on the λ_D , which will invariably overestimate a significant set of beams, mainly due to the flange-lip width ratio and the critical half-wave number influence – this is not a specific disadvantage of the DSM since the traditional “Effective Width Method” (EWM) also does not take into account these two

parameters¹¹. In this work, the second approach is adopted, however, it should be noted that the proposed curves will be strongly affected by the geometries selected/determined in Section 2.

4. Direct Strength Method Design

The Direct Strength Method (DSM), developed by Schafer & Peköz (1998) based on an original idea from Hancock *et al.* (1994), is nowadays universally accepted by the technical/scientific community as an efficient and reliable approach for the design of cold-formed steel members. This is mainly because the member (column or beam) strength against either (i) individual local, distortional and global individual or (ii) interactive failures involving the above buckling phenomena can be accurately predicted on the sole basis of the elastic buckling and yield stresses. For beams with (i) cross-sections symmetric with respect to the bending axis or (ii) cross-sections for which first yield occurs in compressed fibres¹², the currently codified DSM design curve against distortional failures is defined by (AISI 2012)

$$M_{ND} = \begin{cases} M_y + (1 - C_{yd}^{-2})(M_p - M_y) & \lambda_D \leq 0.673 \\ (1 - 0.22\lambda_D^{-0.5})\lambda_D^{-0.5}M_y & \lambda_D > 0.673 \end{cases} \quad (1)$$

where M_{ND} is the beam distortional nominal strength, M_y and M_p are the beam yield and plastic moments, respectively, $\lambda_D = (M_y/M_{crD})^{0.5}$ is the beam distortional slenderness and $C_{yd} = (0.673/\lambda_D)^{0.5} \leq 3$.

Figs. 14(a)-(d) show the variation of M_U/M_y against λ_D for the C-beams (Fig. 14(a)), H_M-beams (Fig. 14(b)), Z-beams (Fig. 14(c)) and H_m-beams (Fig. 10(d)), jointly for the SCA and SCB support conditions¹³. These figures also show (i) the currently codified DSM distortional design curve (M_{ND}/M_y)¹⁴ and (ii) a few proposed DSM-based distortional strength curves. The observation of Fig. 14 shows that:

- (i) Almost all M_U/M_y values are well aligned along a “Winter-type” curve with a small “vertical dispersion” (although more pronounced in the SCB beams – see Section 3.3).
- (ii) As expected, the currently codified DSM distortional design curve provides very substantial failure moments overestimations for beams with moderate-to-high slenderness values ($\lambda_D > 1.25$) even for the SCB-beams – the H_M+BCB M_U/M_y values are those closer to the codified DSM distortional design curve. However, there are a few exceptions: the C2+SCB, H_M2+SCB and Z2+SCB beams ($b_w=150\text{mm}$, $b_f=120\text{mm}$, $b_f=10\text{mm}$, $t=3.50\text{mm}$, $L_C=L_H=550\text{mm}$, $L_Z=700\text{mm}$), whose M_U/M_y values practically coincide with the current DSM predictions – this is explained by the fact that these beams have a flange-lip width ratio equal to 12 (the highest value considered) (see Section 3.4.1). On the other hand, the influence of the inclusion of the rigid end plates (SCA vs. SCB) is more relevant (higher additional strengths) in the H-beams, followed by the Z-beams and the C-beams.

¹¹ The effect of the initial imperfection is not taken into account since all the beams analyzed (2nd-order analysis) contain the worst initial geometric shape. As for effect of beams with the two boundary conditions, it was found out (see Section 3.3) that they cannot be considered jointly – the consideration of these two types of beams must be addressed separately (the implicit consideration of the boundary conditions through the M_{crD} in the DSM distortional curve is not enough).

¹² It is worth noting that the inclusion of the inelastic strength reserve was based on the work of Shifferaw & Schafer (2012). However, these authors analyzed exclusively C and Z beams with boundary conditions similar to the SCB.

¹³ For each beam geometry selected, 17 distinct distortional slenderness values were generated randomly, following a continuously uniform distribution in the interval [0.25, 4]. In this way, the optimization procedure discussed next involves beam slenderness values with the same “weight”, thus avoiding the situation depicted in Fig. 1.

¹⁴ Since the inelastic strength reserve depends on the cross-section plastic moment, and 30 different cross-sections were considered for each beam type, it was decided to include only the extreme cases, *i.e.*, those associated with the minimum and maximum plastic moments. In addition, the determination of the Z-section plastic moments (skew-bending) was made following the procedure described by Dwight (1999).

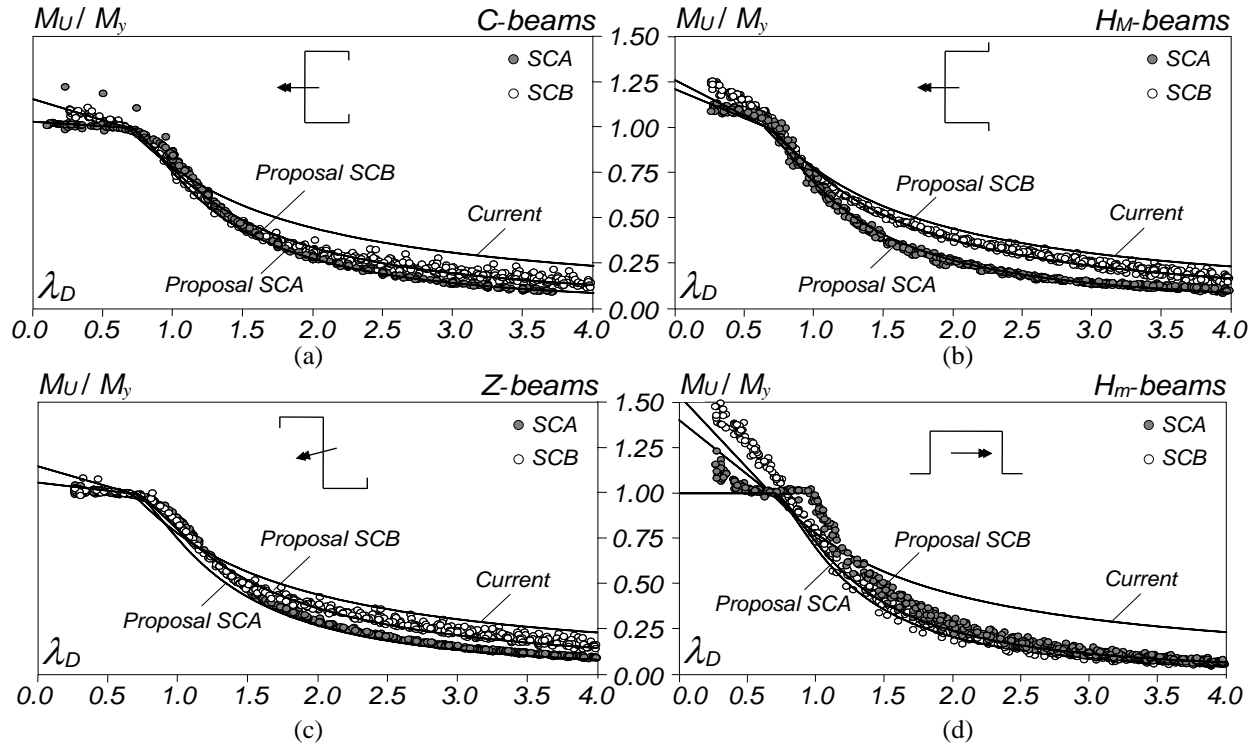


Figure 14: (i) M_U/M_y vs. λ_D plots of (a) C, (b) H_M , (c) Z, and (d) H_m beams, and (ii) current and proposed DSM design curves

- (iii) The observation made in item (iii) of Section 3.3 is confirmed by looking at Fig. 14(a): in the vicinity of $\lambda_D=1.0$, the C+SCB beams exhibit ultimate strength slightly above the C+SCA beam ones – this also applies to the Z-beams (Fig. 14(c)), although to a smaller extent.
- (iv) Figs. 14(a)-(d) clearly show that the consideration of the inelastic strength reserve for $\lambda_D \leq 0.673$, recently included in the AISI (2012), may lead to unsafe designs, particularly for Z-beams. In fact, the work of Shifferaw & Schafer (2012), which is at the root of this design feature, dealt only with C and Z-beams with end support conditions simulating those exhibited by the central beam segment in a 4-point bending test arrangement – “continuous warping”, following somewhere in between the SCA and SCB support conditions (closer to the latter). While the C+BCB beam results (Fig. 14(a)) evidence the presence of an additional strength reserve, the same is not true for their Z-beam counterparts – note that the Z-beams analyzed in the present work have their top flanges uniformly compressed, a more severe situation than that addressed by Shifferaw & Schafer (2012). As for the H_M and H_m beams (SCA and SCB), they exhibit a non-negligible inelastic strength reserve, which is, naturally, higher in the BCB beams.
- (v) Concerning the BCA beams, it can be observed that the M_U/M_y values are fairly well predicted by the elastic buckling curve $(1/\lambda_D)^2$, for $\lambda_D > 1.0$, regardless of the beam type. This is easily explained by the fact that the failure moment is reached almost simultaneously immediately with first yield (no visible elastic-plastic strength reserve is available), making it understandable that the elastic buckling curve provides good estimates of the beam load-carrying capacity.

The currently codified DSM beam distortional design curve is clearly inadequate to estimate failure moments in the moderate-to-high slenderness range and, moreover, beams subjected to major and minor-axis bending cannot be handled jointly. In order to change/improve this situation, and using the failure moment data acquired in this work, it seems possible to make a (preliminary) proposal concerning novel

DSM-based distortional design curves to estimate the failure moments of simply supported cold-formed steel beams under uniform (i) major-axis bending (C and H_M beams), (ii) skew bending (Z beams) and (iii) minor-axis bending (H_m beams). Such curves were obtained by means of the following procedure:

- (i) Definition of the initial plateau, on the basis of the numerical failure moment data concerning the stocky beams, whose collapse is governed exclusively by plasticity (the instability effects are negligible). Based on the results presented in Figs. 14(a)-(d), it was decided to maintain the plateau of the currently codified curve ($\lambda_D=0.673$).
- (ii) Determination of a “Winter-type” curve, cast in the form

$$M_{ND} = \begin{cases} M_y + (1 - C_{yd}^{-2})(M_p - M_y) & \lambda_D \leq 0.673 \\ (1 - a\lambda_D^{-b})\lambda_D^{-c}M_y & \lambda_D > 0.673 \end{cases} \quad (2)$$

through the solution of an optimisation problem defined by

$$\begin{aligned} & \min f(\mathbf{x}) \\ \text{s.a. : } & \left. \frac{M_{ND}}{M_y} \right|_{\lambda_D=0.673} = 1 \\ & \left. \frac{dM_{ND}}{d\lambda_D} \right|_{\lambda_D=0.673} \leq 0 \\ & \frac{1}{N} \sum_{i=1}^N \frac{M_{U,i}}{M_{ND,i}} \geq 0.90 \\ & \min \left(\frac{M_{U,i}}{M_{ND,i}} \right) \geq d \\ & a, b, c, d \geq 0 \end{aligned} \quad (3)$$

where the design variable vector $\mathbf{x} = [a, b, c]$, whose components are the 3 unknowns¹⁵ defining the “Winter-type” curve, $M_{ND} = (1 - a\lambda_D^{-b})\lambda_D^{-c}M_y$ and the objective function reads

$$f(\mathbf{x}) = \sum_{i=1}^N \left(\frac{M_{ND,i}}{M_{y,i}} - \frac{M_{U,i}}{M_{y,i}} \right)^2 \quad (4)$$

here $M_{U,i}$ and $M_{ND,i}$ are the i^{th} numerical failure moment and corresponding DSM estimate, $M_{y,i}$ is the i^{th} elastic bending moment and N is the total number of numerical failure moments for beams with $\lambda_D > 0.673$. Note that the equality constraint in (2) is required to fulfil the criterion given in item (i). Moreover, the first inequality constraint in (2), associated with the derivative of M_{ND} with respect to λ_D , is intended to ensure a decreasing monotonic function (not necessary if $b=c$). Finally, the remaining inequalities in (2) are imposed to avoid excessively unsafe failure moment predictions, even at the cost of a higher objective function value (*i.e.*, higher differences between the curve and numerical failure moments). Depending on the beam type, $d=0.85$ or $d=0.90$ was adopted.

¹⁵ The currently codified DSM beam distortional curve (see eq. (1)) has only two parameters ($b=c$). However, it was concluded that an expression with three parameters yields better results, which explains why such expression is employed in this work.

(iii) The above optimization problem corresponds to a simple multivariable constrained minimization problem with continuous variables, which can be solved employing any classical technique (with or without derivatives) – the discussion of such methods is beyond the scope of this work.

Table 7 provides the solution of the minimization defined in (3), *i.e.*, the values of the unknowns a , b , c associated with the DSM distortional beam strength curves proposed for each combination of (i) beam type (cross-section shape and bending axis) and (ii) end support conditions – between parentheses are indicated the unknown rounded values adopted (note that the corresponding strength curves have already been depicted in Figs. 14(a)-(d). Moreover, Figs. 15(a)-(d) plot, against λ_D , the M_U/M_{ND} values concerning the C, H_M , Z and H_m beams, respectively – each figure contain SCA and SCB values. The observation of the results presented in Table 7 and Figs. 15(a)-(d) prompts the following remarks:

(i) Figs. 15(a)-(d) clearly show the improvement in failure moment prediction achieved by the proposed design curves, along the whole distortional slenderness range considered, as reflected by the M_U/M_{ND}

Table 7: Values of the unknowns concerning the proposed DSM beam distortional strength curves

	SCA			SCB		
	a	b	c	a	b	c
C-beams	0.2468 (0.25)	1.7592 (1.75)	1.7274 (1.75)	0.2363 (0.23)	1.5502 (1.55)	1.4488 (1.45)
H_M -beams	0.2937 (0.30)	1.3041 (1.30)	1.7113 (1.70)	0.2320 (0.23)	1.2962 (1.30)	1.2385 (1.25)
Z-beams	0.2477 (0.25)	1.7567 (1.75)	1.7339 (1.75)	0.1980 (0.20)	1.8254 (1.80)	1.3238 (1.35)
H_m -beams	0.2741 (0.27)	1.6831 (1.70)	1.9268 (1.92)	0.2963 (0.30)	1.6222 (1.60)	2.0915 (2.10)

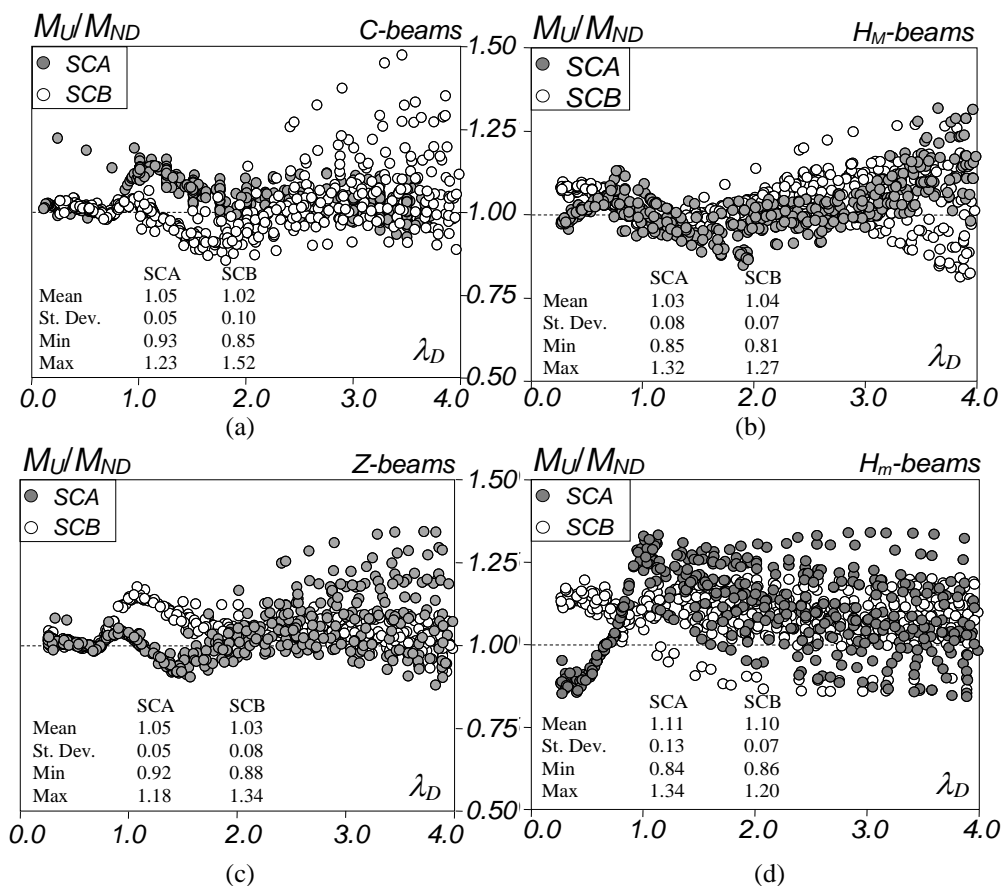


Figure 15: Plots of M_U/M_{ND} against λ_D for the (a) C, (b) H_M , (c) Z and (d) H_m beams with SCA and SCB support conditions

indicators: mean values close to 1.00 and low standard deviations (not exceeding 10%, value obtained for the C+BCB beams). Naturally, there are a few overly safe estimates, associated with the beams with large flange-lip width ratios (see Section 3.4.1). On the other hand, the unsafe estimates concern the low flange-lip width ratios, *e.g.*, H_m17 and H_m18 SCA beams (see Fig. 15(d)).

- (ii) Table 7 shows that the strength curves obtained for the C and Z SCA beams are identical – the curve for the H_M+SCA beams stems from a slightly lower *b* value. Moreover, the differences between the curves obtained for the various SCB beam types are higher (distinct elastic-plastic strength reserves).

Since the DSM design approach associated with a specific ultimate limit state require the definition of a “cross-section domain of application” (the so-called “pre-qualified cross-sections”), the next step is to identify which beam types can be designed by means of a given strength curve. It was found that the failure moments of the C, H_M and Z beams with the same end support conditions (SCA or SCB) may be estimated through a single design curve, as discussed below – the H_m beams must be handled separately. Figs. 16(a)-(b) plot, against λ_D , the M_U/M_y values concerning the C, H_M and Z-beams with (i) SCA and (ii) SCB support conditions – recall the final strength curves concerning the H_m beams were already presented (see Table 7 and Fig. 14(d)). Once again, the “best design curves” were obtained from the solution of the optimization/minimization problem defined in (3), now involving jointly three beam types – the curves determined are also depicted in Figs. 16(a)-(b), where the corresponding *a*, *b*, *c* values are given. Finally, Figs. 17(a)-(b) (joining results included in Figs. 15(a)-(c)) plot, against λ_D , the M_U/M_{ND} values concerning the three beam types. The observation of these figures shows that:

- (i) The M_U/M_{ND} indicators are now, obviously, more conservative than those obtained earlier. The DSM design curve for SCA beams is governed, in the low-to-moderate distortional slenderness range, by the H_M beam failure moment predictions – there are only small differences between the predictions concerning the three types of slender beams. On the other hand, the C beam failure moment estimates govern the SCB DSM design curve in the moderate-to-high distortional slenderness range.
- (ii) The “vertical dispersion” is much more pronounced for the SCB beams, due to the different inelastic strength reserve exhibited by various beam types – such strength reserve is absent in all SCA beams.
- (iii) The proposed DSM design/strength curves are more adequate than the codified one to estimate the failure moments of simply supported beams failing in distortional modes. However, the authors recognize that there is a (natural) dependence on the cross-section dimensions and length (through the critical buckling mode half-wave number) that cannot be explicitly accounted by the DSM without “soiling” its roots and elegance, because such dependence cannot be captured solely by the distortional slenderness – this implies unavoidable beam failure moment excessive underestimations.

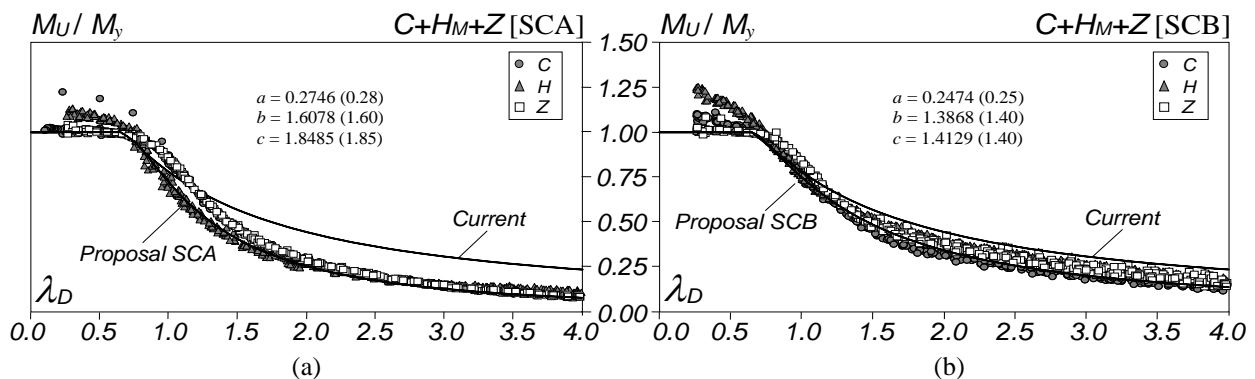


Figure 16: (i) M_U/M_y vs. λ_D plots of the C, H_M, Z beams with (a) SCA and (b) SCB support conditions, and current and proposed DSM beam distortional design curves

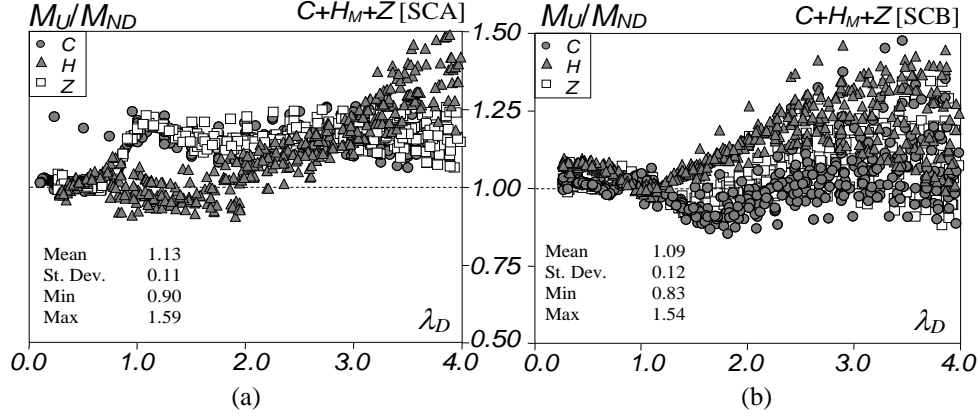


Figure 17: Plots of M_U/M_{ND} against λ_D for the C, H_M , Z beams with (a) SCA and (b) SCB support conditions

Lastly, Fig. 18(a) revisits Fig. 1 and adds the two design curves proposed in this work, thus enabling to compare the quality of their predictions with that of the current strength curve. Fig. 18(b), on the other hand, plots, against the λ_D , the experimental and numerical failure moments obtained by Yu & Schafer (2006) and already mentioned in Section 1. The observation of these results shows that:

- (i) The overwhelming majority of the tests results considered to calibrate the current M_{ND} strength curve are also fairly well predicted by the two proposed curves, even if a bit more on the safe side for $\lambda_D > 1.0$ (see Fig. 18(a)). As pointed out earlier, most of these test results concern rather stocky beams, for which there are very little differences between the failure moment predictions provided by the current and proposed (for SCA and SCB beams) – recall that the beam segments involved in the four-point bending tests exhibited “warping continuity” at their end cross-section, while the proposed design curves were developed in the context of simply supported beams whose end cross-sections had warping either completely free or fully prevented.
- (ii) Moreover, the two proposed curves underestimate considerably the failure moments yields very of a small number of reasonably slender beams, as shown in Fig. 18(a) – this may be due to the bracing arrangement adopted in the tests which, according to Schafer (2008), “typically restrained distortional buckling in part, but not necessarily in full”, thus leading to higher failure moments.
- (iii) By looking at Fig. 18(b), it is readily recognized that the two proposed design curves underestimate a large fraction of the results reported by Yu & Schafer (2006) by larger margins than the currently codified strength curve. However, none of these results concerns beams with slenderness above 1.5, a range for which the current strength curve has been shown to be inadequate.

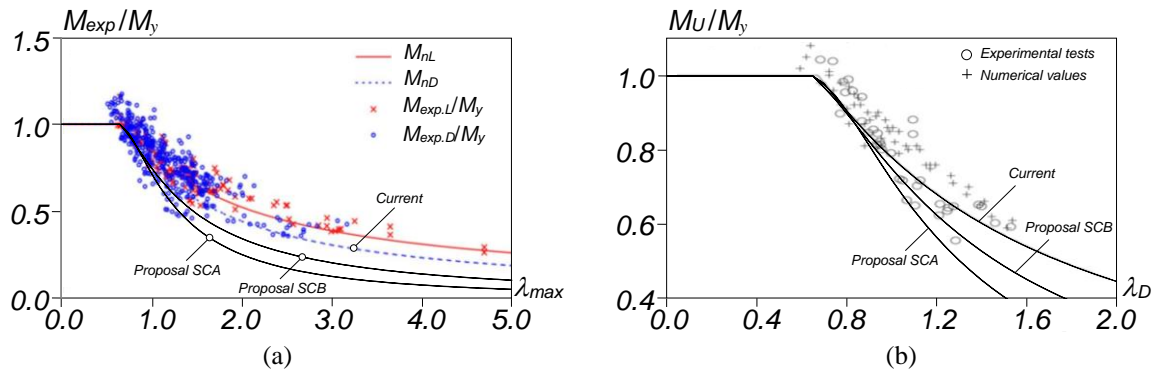


Figure 18: DSM beam distortional design curves (current and proposed) and experimental distortional failure moments (a) used to develop the current strength curve (b) reported by Yu & Schafer (2006) (both figures adapted from Schafer 2008)

5. Conclusion

A numerical investigation on the distortional post-buckling behavior, ultimate strength and DSM design of simply supported cold-formed steel beams subjected to uniform bending was reported. The beams analyzed had three cross-section shapes and different bending axes, namely (i) lipped channels (major-axis bending), (ii) hat-sections (major and minor-axis bending) and (iii) zed-sections (skew bending causing uniform flange compression – worst case). Moreover, the beams analyzed exhibited (i) two simply supported conditions (SCA and SCB), differing in the warping and local displacement/rotation restraints, (ii) several yield stresses, intended to cover a wide distortional slenderness range, and (iii) various cross-section dimensions ratios and lengths, to assess their influence on the distortional post-buckling behavior and ultimate strength.

Initially, a beam geometry selection procedure was presented, aimed at identifying simply supported beams buckling and failing in distortional modes. Then, the elastic and elastic-plastic (distortional) post-buckling behaviors of several beams were investigated, in order to (i) determine the most detrimental initial imperfection shape, (ii) assess the effect of the two end support conditions considered (SCA and SCB), (iii) investigate the influence of the cross-section dimensions, namely the flange-lip and web-flange width ratios, and (iv) to assess the impact of the critical buckling mode half-wave number. Then, an extensive parametric study was carried out, by means of non-linear (materially and geometrically) shell finite element ABAQUS analyses, aimed at gathering beam distortional failure moment data intended to be used in assessing the quality of their estimates provided by the currently codified DSM beam distortional design curve. Since this assessment revealed poor quality estimates, particularly for slender beams, additional research was devoted to developing/proposing novel DSM distortional strength curves able to cover all the beams analyzed in this work.

Among the various findings reported in this paper, the following ones deserve to be specially mentioned:

- (i) The distortional initial imperfections involving inward compressed flange-lip motions are the most detrimental in the lipped channel and Hat-section beams bent about the major-axis, as well as in the Zed-section beams bent to exhibit a neutral axis parallel to the flanges. However, in the Hat-section beams bent about the minor-axis the most detrimental initial imperfections involving outward flange-lip motions (both flange-lip assemblies are compressed). Note that this distortional post-buckling asymmetry is only relevant for beams buckling in modes with odd half-wave numbers.
- (ii) The end support conditions, flange-lip width ratio and the critical buckling mode half-wave number play important roles in the distortional post-buckling ultimate strength of all the beams analyzed in this work. Moreover, roles played by the flange-lip width ratio and critical buckling mode half-wave number were found to be more relevant in the BCB beams.
- (iii) The elastic and elastic-plastic distortional post-buckling behaviors of SCA and SCB beams with the same geometry and yield stress are clearly distinct in stiffness and strength. In particular, unlike SCB beams, non-stocky SCA beams exhibit practically no elastic-plastic strength reserve, which explains why their failure moments are fairly well predicted by the elastic buckling strength curve.
- (iv) The currently codified DSM distortional design curve is unable to predict adequately the failure moments of the simply supported beams analyzed in this work. Indeed, it provides excessively unsafe estimates for the non-stocky beams, thus, confirming and extending the recent findings of Landesmann & Camotim (2016), in the context of lipped channel beams under major-axis bending.
- (v) Several DSM distortional design curves were proposed and shown to perform much better than the current one for SCA and SCB simply supported beams. Such curves cover beams under (v_1) major-axis bending (lipped channels and hat-sections), (v_2) skew bending (zed-sections) and (v_3) minor-

axis bending (hat-sections). Although the DSM cannot capture the dependence of the failure moment on beam cross-section dimension ratios and buckling mode half-wave number, without including those parameters explicitly in the strength curve expressions, it was found that it is still possible to predict them on the sole basis of the distortional slenderness – obviously, the “price” to pay is the fact that some beam failure moments are severely underestimated by the proposed design curves.

- (vi) The two proposed design curves provide fairly accurate (and practically always safe) estimates of the beam failure moments used to develop and calibrate the current distortional strength curve, and also those later reported by Yu & Schafer (2006). However, since the above failure moments involve only non-slender beams ($\lambda_D \leq 1.5$) and the open questions concern essentially the moderate-to-high slenderness range, there is a clear need for a test campaign focusing on slender beams.

Finally, one last word to mention that the authors are currently working on extending the study reported in this paper to simply supported beams under non-uniform bending, thus extending the work of Bebiano *et al.* (2007), in order to investigate the DSM-based prediction of their distortional failure moments.

Acknowledgments

The first author gratefully acknowledges the financial support of FCT (*Fundação para a Ciência e a Tecnologia* – Portugal), through the doctoral scholarship SFRH/BD/87746/2012.

References

- American Iron and Steel Institute (AISI) (2012). *North American Specification (NAS) for the Design of Cold-Formed Structural Members*, AISI-S100-12, Washington DC.
- Bebiano, R, Pina, P, Silvestre, N, Camotim, D (2008). *GBTUL 1.0 β – Buckling and Vibration Analysis of Thin-Walled Members*, University of Lisbon (formerly Technical University of Lisbon), <http://www.civil.ist.utl.pt/gbt>.
- Bebiano R, Dinis PB, Silvestre N, Camotim D (2007). “On the application of the direct strength method to cold-formed steel beams subjected to non-uniform bending”, *Proceedings of 5th International Conference on Advances in Steel Structures (ICASS 2007, Singapore 5-7/12)*, J.Y.R. Liew, Y.S. Choo (eds.), Research Publishing (Singapore), 322-327 (vol. III).
- Bernard ES, Bridge RQ, Hancock GJ (1996). “Flange curling in profiled steel decks”, *Thin-Walled Structures*, **25**(1), 1-29.
- Camotim D, Dinis PB (2013). “Distortional-global interaction in lipped channel columns”, *Proceedings of the Institution of Civil Engineers (ICE)-Structures and Buildings*, **166**(8), 381-391.
- Dinis PB, Camotim D (2010). “Local/distortional mode interaction in cold-formed steel lipped channel beams”, *Thin-Walled Structures*, **48**(10-11), 771-785.
- Dwight J (1999). *Aluminium Design and Construction*, Routledge, New York.
- Hancock GJ, Kwon YB, Bernard ES (1994). “Strength design curves for thin-walled sections undergoing distortional buckling”, *Journal of Constructional Steel Research*, **31**(2-3), 169-186.
- Landesmann A, Camotim D (2016). “Distortional failure and DSM design of cold-formed steel lipped channel beams under elevated temperatures”, *Thin-Walled Structures*, **98A** (January), 75-93.
- Martins AD, Dinis PB, Camotim D, Providência P (2015). “Local-distortional interaction in pin-ended lipped channel beams: behaviour, strength and DSM design”, CD-ROM *Proceedings of 8th International Conference on Advances in Steel Structures (ICASS 2015 – Lisbon, 21-24/7)*, D. Camotim *et al.* (eds.), Paper 15.
- Martins AD, Camotim D, Dinis PB (2016). “On the DSM design of cold-formed steel beams experiencing local-distortional interaction”, *Proceedings of 6th International Conference on Structural Engineering, Mechanics and Computation (SMEC 2016 – Cape Town, 5-7/9)*. (in press)
- Prola LC, Camotim D (2002). “On the distortional post-buckling behaviour of cold-formed lipped channel steel beams”, *Advances in Steel Structures (ICASS’02 – Hong Kong, 9-11/12)*, S.L. Chan, J.G. Teng, K.F. Chung (eds.), Elsevier (Amsterdam), 331-339 (vol. 1).
- Schafer BW (2008). “Review: the direct strength method of cold-formed member design”, *Journal of Constructional Steel Research*, **64**(7-8), 766-778.

- Schafer BW, Peköz T (1998). "Direct strength prediction of cold-formed steel members using numerical elastic buckling solutions", *Proceedings of 14th International Specialty Conference on Cold-Formed Steel Structures* (St. Louis, 15-16/10), W.W. Yu, R. Laboube (eds.), 69-76.
- Shifferaw Y, Schafer BW (2012). "Inelastic bending capacity of cold-formed steel members", *Journal of Structural Engineering* (ASCE), **138**(4), 468-480.
- Silvestre, N, Bebiano, R, Camotim, D (2005). "On the distortional post-buckling asymmetry of cold-formed steel channel columns with different stiffener configurations", *USB Proceedings of the SSRC Annual Stability Conference* (Montreal, Canada 6-9/04).
- Simulia Inc. (2009). *ABAQUS Standard* (version 6.9-3).
- Wang L, Young B (2014). "Design of cold-formed steel channel with stiffened webs subjected to bending", *Thin-Walled Structures*, **85** (December), 81-92.
- Yu C, Schafer BW (2003). "Local buckling tests on cold-formed steel beams", *Journal of Structural Engineering* (ASCE), **129**(12), 1596-1606.
- Yu C, Schafer BW (2006). "Distortional buckling tests on cold-formed steel beams", *Journal of Structural Engineering* (ASCE), **132**(4), 515-528.
- Yu C, Schafer BW (2007). "Simulation of cold-formed steel beams in local and distortional buckling with applications to the direct strength method", *Journal of Constructional Steel Research*, **63**(5), 581-590.

ANNEX A – DATA CONCERNING THE SELECTED BEAMS

Table A.1: Selected lipped channel beams failing in “pure” distortional modes under major-axis bending: geometry, buckling moments and their relevant moment ratios (dimensions in mm and moments in kNm)

	b_w	b_f	b_l	t	$\frac{b_w}{b_f}$	$\frac{b_f}{b_l}$	SCA				SCB			
							L	M_{crD}	$\frac{M_{crL}}{M_{crD}}$	$\frac{M_{crG}}{M_{crD}}$	L	M_{crD}	$\frac{M_{crL}}{M_{crD}}$	$\frac{M_{crG}}{M_{crD}}$
C1	120	75	10	3.00	1.60	7.5	320	1788	2.7	39	500	2580	2.0	25
C2	150	120	10	3.50	1.25	12.0	420	1905	2.8	106	550	2857	3.0	93
C3	160	100	10	2.20	1.60	10.0	460	842	2.2	86	700	1236	1.6	57
C4	200	100	10	2.50	2.00	10.0	450	1393	2.5	82	700	2013	1.9	53
C5	210	70	9	2.50	3.00	7.8	340	1954	2.2	44	550	2750	2.3	27
C6	210	110	10	2.50	1.91	11.0	500	1314	2.5	95	800	1883	1.8	0
C7	150	95	10	2.50	1.58	9.5	400	1126	2.3	79	700	1620	1.8	40
C8	150	100	10	2.50	1.50	10.0	450	1062	2.4	75	750	1528	1.7	42
C9	150	75	10	2.50	2.00	7.5	400	1468	2.4	34	600	2090	1.8	24
C10	150	80	10	2.50	1.88	8.0	400	1359	2.5	43	600	1960	1.8	30
C11	130	80	10	3.00	1.63	8.0	350	1803	2.6	42	500	2619	2.0	32
C12	130	80	10	3.00	1.63	8.0	400	1848	2.5	32	550	2583	2.0	27
C13	140	90	10	2.50	1.56	9.0	350	1145	2.3	81	650	1617	1.8	38
C14	145	90	10	2.45	1.61	9.0	450	1115	2.4	52	675	1594	1.7	36
C15	150	100	10	2.50	1.50	10.0	450	1062	2.4	75	725	1531	1.8	45
C16	120	80	10	2.50	1.50	8.0	350	1101	2.4	71	600	1593	1.7	28
C17	130	80	10	2.50	1.63	8.0	400	1193	2.4	41	600	1716	1.8	28
C18	130	80	10	2.50	1.63	8.0	500	1331	2.2	23	550	1735	1.7	33
C19	135	75	10	2.70	1.80	7.5	300	1602	2.4	52	550	2262	1.9	25
C20	135	85	10	2.80	1.59	8.5	350	1493	2.6	58	600	2143	1.9	31
C21	135	90	10	2.80	1.50	9.0	450	1453	2.3	41	650	2013	1.9	35
C22	125	80	10	2.90	1.56	8.0	300	1639	2.4	58	500	2345	2.0	33
C23	125	80	10	2.90	1.56	8.0	400	1655	2.4	32	550	2309	1.9	28
C24	160	90	10	2.50	1.78	9.0	400	1267	2.5	66	700	1824	1.8	34
C25	165	85	10	2.40	1.94	8.5	400	1261	2.5	58	675	1821	1.8	32
C26	250	100	12	2.80	2.50	8.3	500	2591	2.4	56	850	3713	1.8	31
C27	275	110	13	3.00	2.50	8.5	550	3204	2.4	58	600	5502	2.2	65
C28	265	105	13	3.00	2.52	8.1	550	3253	2.4	49	650	5144	2.4	50
C29	215	80	10	2.80	2.69	8.0	400	2477	2.5	42	625	3489	2.0	27
C30	225	90	12	2.90	2.50	7.5	450	2845	2.5	44	775	4079	1.8	23

Table A.2: Selected hat-section beams failing in “pure” distortional modes under major-axis bending: geometry, buckling moments and their relevant moment ratios (dimensions in mm and moments in kNcm)

←	b_w	b_f	b_l	t	$\frac{b_w}{b_f}$	$\frac{b_f}{b_l}$	SCA				SCB			
							L	M_{crD}	$\frac{M_{crL}}{M_{crD}}$	$\frac{M_{crG}}{M_{crD}}$	L	M_{crD}	$\frac{M_{crL}}{M_{crD}}$	$\frac{M_{crG}}{M_{crD}}$
H1	120	75	10	3.00	1.60	7.5	320	1672	3.6	38	450	2441	2.5	29
H2	150	120	10	3.50	1.25	12.0	420	1828	3.9	104	550	2708	2.7	91
H3	160	100	10	2.20	1.60	10.0	460	808	2.8	85	650	1202	1.9	64
H4	200	100	10	2.50	2.00	10.0	450	1354	3.2	81	550	2120	2.0	77
H5	210	70	9	2.50	3.00	7.8	340	1929	2.6	43	550	2682	1.9	26
H6	210	110	10	2.50	1.91	11.0	500	1278	3.2	94	600	1979	2.1	94
H7	150	95	10	2.50	1.58	9.5	400	1078	3.1	77	550	1627	2.0	60
H8	150	100	10	2.50	1.50	10.0	450	1014	3.1	74	600	1504	2.1	62
H9	150	75	10	2.50	2.00	7.5	400	1392	3.2	33	450	2149	2.0	37
H10	150	80	10	2.50	1.88	8.0	400	1291	3.1	42	500	1942	2.1	39
H11	130	80	10	3.00	1.63	8.0	350	1696	3.6	41	450	2528	2.4	37
H12	130	80	10	3.00	1.63	8.0	400	1740	3.5	40	550	2395	2.5	26
H13	140	90	10	2.50	1.56	9.0	350	1096	3.0	79	550	1581	2.1	49
H14	145	90	10	2.45	1.61	9.0	450	1056	3.0	51	550	1574	2.0	51
H15	150	100	10	2.50	1.50	10.0	450	1014	3.1	74	600	1504	2.1	62
H16	120	80	10	2.50	1.50	8.0	350	1033	3.1	50	500	1539	2.1	37
H17	130	80	10	2.50	1.63	8.0	400	1119	3.1	40	500	1672	2.1	38
H18	130	80	10	2.50	1.63	8.0	500	1232	2.8	36	600	1598	2.2	28
H19	135	75	10	2.70	1.80	7.5	300	1526	3.3	50	450	2234	2.2	34
H20	135	85	10	2.80	1.59	8.5	350	1417	3.4	56	450	2199	2.2	48
H21	135	90	10	2.80	1.50	9.0	450	1364	3.3	41	500	1995	2.2	50
H22	125	80	10	2.90	1.56	8.0	300	1554	3.4	56	450	2265	2.3	38
H23	125	80	10	2.90	1.56	8.0	400	1539	3.4	57	550	2137	2.5	27
H24	160	90	10	2.50	1.78	9.0	400	1215	3.1	65	550	1816	2.1	51
H25	165	85	10	2.40	1.94	8.5	400	1212	3.0	57	550	1808	2.1	45
H26	200	100	10	3.00	2.00	10.0	420	2075	3.7	73	500	3225	2.4	73
H27	200	95	10	3.00	2.11	9.5	410	2196	3.7	63	450	3586	2.2	71
H28	200	90	10	3.00	2.22	9.0	400	2330	3.6	55	450	3706	2.3	60
H29	210	90	10	3.00	2.33	9.0	400	2449	3.6	56	450	3908	2.3	61
H30	210	80	10	3.00	2.63	8.0	370	2781	3.3	43	550	3903	2.4	31

Table A.3: Selected zed-section beams failing in “pure” distortional modes under skew bending: geometry, buckling moments and their relevant moment ratios (dimensions in mm and moments in kNcm)

	b_w	b_f	b_l	t	$\frac{b_w}{b_f}$	$\frac{b_f}{b_l}$	SCA				SCB			
							L	M_{crD}	$\frac{M_{crL}}{M_{crD}}$	$\frac{M_{crG}}{M_{crD}}$	L	M_{crD}	$\frac{M_{crL}}{M_{crD}}$	$\frac{M_{crG}}{M_{crD}}$
Z1	120	75	10	3.00	1.60	7.5	500	2216	2.4	11	525	2951	2.0	17
Z2	150	120	10	3.50	1.25	12.0	500	2445	2.8	45	700	3323	2.0	39
Z3	160	100	10	2.50	1.60	10.0	450	1286	2.4	57	725	1854	1.8	35
Z4	200	100	10	2.50	2.00	10.0	450	1509	2.5	69	750	2166	1.8	39
Z5	210	70	9	2.50	3.00	7.8	400	2082	2.5	29	575	2830	1.9	23
Z6	210	110	10	2.50	1.91	11.0	500	1435	2.5	79	825	2053	1.8	43
Z7	150	95	10	2.50	1.58	9.5	400	1290	2.4	58	700	1857	1.8	30
Z8	150	100	10	2.50	1.50	10.0	450	1235	2.4	54	725	1779	1.8	33
Z9	150	75	10	2.50	2.00	7.5	400	1600	2.4	28	600	2276	1.8	20
Z10	150	80	10	2.50	1.88	8.0	400	1498	2.5	35	525	2217	1.7	26
Z11	130	80	10	3.00	1.63	8.0	600	2092	2.5	11	500	2986	2.0	24
Z12	130	80	10	3.00	1.63	8.0	400	2140	2.4	23	550	2949	2.0	20
Z13	140	90	10	2.50	1.56	9.0	400	1286	2.4	47	650	1863	1.8	28
Z14	145	90	10	2.45	1.61	9.0	400	1257	2.4	50	675	1819	1.7	27
Z15	150	100	10	2.50	1.50	10.0	450	1235	2.4	54	700	1782	1.8	35
Z16	120	80	10	2.50	1.50	8.0	400	1292	2.4	28	600	1864	1.7	20
Z17	130	80	10	2.50	1.63	8.0	400	1365	2.4	30	600	1959	1.8	21
Z18	290	150	14	2.90	1.93	10.7	750	2589	2.3	80	1100	3787	1.6	36
Z19	135	75	10	2.70	1.80	7.5	400	1806	2.4	23	550	2546	1.9	19
Z20	135	85	10	2.80	1.59	8.5	400	1731	2.5	32	600	2459	1.9	23
Z21	135	90	10	2.80	1.50	9.0	400	1639	2.5	39	625	2346	1.9	25
Z22	125	80	10	2.90	1.56	8.0	600	1891	2.4	11	550	2666	1.9	20
Z23	300	135	14	2.90	2.22	9.6	700	2929	2.3	67	1100	4247	1.7	33
Z24	160	90	10	2.50	1.78	9.0	400	1409	2.5	53	675	2034	1.8	29
Z25	165	85	10	2.40	1.94	8.5	400	1377	2.5	48	650	1995	1.8	28
Z26	250	100	12	2.50	2.50	8.3	550	2097	2.2	48	900	3023	1.6	28
Z27	275	110	13	2.90	2.50	8.5	550	3112	2.4	55	950	4464	1.7	29
Z28	265	105	13	2.90	2.52	8.1	550	3152	2.3	46	900	4539	1.7	27
Z29	215	80	10	2.60	2.69	8.0	400	2159	2.5	42	650	3066	2.1	25
Z30	225	90	12	2.80	2.50	7.5	450	2760	2.4	41	775	3967	1.8	22

Table A.4: Selected hat-section beams failing in “pure” distortional modes under minor-axis bending: geometry, buckling moments and their relevant moment ratios (dimensions in mm and moments in kNcm)

	b_w	b_f	b_l	t	$\frac{b_w}{b_f}$	$\frac{b_f}{b_l}$	SCA				SCB			
							L	M_{crD}	$\frac{M_{crL}}{M_{crD}}$	$\frac{M_{crG}}{M_{crD}}$	L	M_{crD}	$\frac{M_{crL}}{M_{crD}}$	$\frac{M_{crG}}{M_{crD}}$
H1	100	70	10	1.50	1.43	7.0	600	173	4.2	9	700	235	3.1	18
H2	100	60	12	1.50	1.67	5.0	600	207	3.8	5	700	292	2.7	11
H3	120	60	12	1.50	2.00	5.0	600	199	3.9	12	700	287	2.7	16
H4	130	55	12	1.50	2.36	4.6	600	206	3.7	8	700	282	2.6	16
H5	80	55	12	1.50	1.45	4.6	500	202	3.9	4	700	300	2.6	6
H6	80	55	10	1.30	1.45	5.5	400	118	4.3	10	500	200	2.5	14
H7	90	80	15	1.70	1.13	5.3	700	321	3.8	4	900	491	2.4	6
H8	90	70	15	1.70	1.29	4.7	600	315	3.7	4	950	486	2.4	4
H9	110	70	13	1.70	1.57	5.4	700	299	3.8	5	900	399	2.8	9
H10	110	60	12.5	1.70	1.83	4.8	600	283	4.0	5	700	389	2.9	11
H11	120	70	12	1.60	1.71	5.8	700	241	3.8	7	800	321	2.9	16
H12	125	75	13	1.75	1.67	5.8	750	317	3.8	7	900	416	2.9	13
H13	130	75	14	1.75	1.73	5.4	800	343	3.6	7	900	451	2.8	13
H14	80	100	15	1.85	0.80	6.7	650	373	4.2	5	900	606	2.6	6
H15	90	90	15	1.85	1.00	6.0	750	389	4.0	4	800	621	2.5	8
H16	95	65	15	1.90	1.46	4.3	600	412	3.8	4	800	608	2.6	5
H17	105	50	16	2.20	2.10	3.1	500	587	3.2	3	700	846	2.2	4
H18	120	60	18	2.30	2.00	3.3	650	744	3.1	3	850	1040	2.2	4
H19	135	80	18	2.30	1.69	4.4	850	775	3.6	4	1000	1039	2.7	7
H20	140	85	20	2.40	1.65	4.3	950	953	3.3	3	1200	1259	2.5	5
H21	200	130	25	2.70	1.54	5.2	1500	1495	3.1	4	1700	1934	2.4	9
H22	200	150	25	2.70	1.33	6.0	1600	1444	3.2	5	2000	1915	2.4	9
H23	200	170	25	2.70	1.18	6.8	1700	1404	3.3	6	2000	1906	2.4	11
H24	220	150	30	3.00	1.47	5.0	1700	2112	3.0	4	2200	2885	2.3	7
H25	300	200	30	3.00	1.50	6.7	2200	2018	3.0	8	2500	2713	2.2	13
H26	250	200	30	3.00	1.25	6.7	2200	2141	2.9	5	2500	2790	2.2	12
H27	250	150	25	2.70	1.67	6.0	1700	1429	3.1	7	2000	1848	2.4	15
H28	175	120	17.5	2.00	1.46	6.9	1200	522	3.4	9	1500	706	2.5	16
H29	165	100	17.5	2.00	1.65	5.7	1100	554	3.3	6	1250	725	2.5	14
H30	100	110	17.5	2.20	0.91	6.3	850	632	4.1	4	1000	1000	2.6	7